

1   **The impact of aerosols on photolysis frequencies and ozone**  
2   **production in urban Beijing during the four-year period**  
3   **2012–2015**

4   Wenjie Wang<sup>1</sup>, Min Shao<sup>1,2\*</sup>, Min Hu<sup>1</sup>, Limin Zeng<sup>1</sup>, Yusheng Wu<sup>1</sup>

5

6   1 State Joint Key Laboratory of Environmental Simulation and Pollution Control,  
7   College of Environmental Sciences and Engineering, Peking University, Beijing  
8   100871, China

9   2 Institute for Environmental and Climate Research, Jinan University, Guangzhou  
10   511443, China

11

12

13

14

15

16

17   **\* Correspondence to:**

18   Prof. Min SHAO

19   College of Environmental Sciences and Engineering, Peking University, Beijing  
20   100871, China

21   Tel: +86-10-62757973; Fax: +86-10-62757973

22   Email: mshao@pku.edu.cn

23      **Abstract**

24      During the period 2012-2015, the photolysis frequencies were measured at the  
25      Peking University site (PKUERS), a representative site of urban Beijing. We present a  
26      study of the effects of aerosols on two key photolysis frequencies,  $j(O^1D)$  and  $j(NO_2)$ .  
27      Both  $j(O^1D)$  and  $j(NO_2)$  display significant dependence on AOD (380nm) with a  
28      nonlinear negative correlation. With the increase in AOD, the slopes of photolysis  
29      frequencies vs AOD decrease, which indicates that the capacity of aerosols to reduce  
30      the actinic flux decreases with AOD. The absolute values of slopes are equal to  
31       $4.2\text{-}6.9 \cdot 10^{-6} \text{ s}^{-1}$  and  $3.2\text{-}10^{-3} \text{ s}^{-1}$  per AOD unit for  $j(O^1D)$  and  $j(NO_2)$  respectively at  
32      SZA of  $60^\circ$  and AOD smaller than 0.7, both of which are larger than those observed  
33      in a similar, previous study in the Mediterranean. This indicates that the aerosols in  
34      urban Beijing have a stronger extinction effect on actinic flux than absorptive dust  
35      aerosols in the Mediterranean. Since the photolysis frequencies strongly depended on  
36      the AOD and the solar zenith angle (SZA), we established a parametric equation to  
37      quantitatively evaluate the effect of aerosols on photolysis frequencies in Beijing.  
38      According to the parametric equation, aerosols lead to a decrease in seasonal mean  
39       $j(NO_2)$  by 24% and 30% for summer and winter, respectively, and the corresponding  
40      decrease in seasonal mean  $j(O^1D)$  by 27% and 33% respectively, compared to an  
41      aerosol-free atmosphere ( $AOD = 0$ ). Based on an observation campaign in August  
42      2012, we used the photochemical box model to simulate the ozone production rate  
43      ( $P(O_3)$ ). The simulation results shows that the monthly mean daytime net ozone  
44      production rate is reduced by up to 25% due to the light extinction of aerosols.

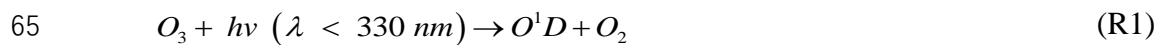
45 Through further in-depth analysis, it was found that particulate matter concentrations  
46 maintain high level under the condition of high concentrations of ozone precursors  
47 (VOCs and NO<sub>x</sub>), which inhibits the production of ozone to a large extent. This  
48 phenomenon implies a negative feedback mechanism in the atmospheric environment  
49 of urban Beijing.

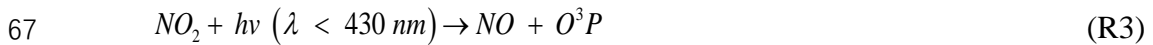
50

51

52 **1. Introduction**

53 Solar radiation plays an important role in atmospheric photochemistry, driving  
54 the photolysis of many key species. The photolysis of ozone (O<sub>3</sub>), gaseous nitrous  
55 acid (HONO), and carbonyl species, which contributes to the primary production of  
56 HO<sub>x</sub> (Volkamer et al., 2010). The photolysis of ozone produces O<sup>1</sup>D, which then  
57 reacts with H<sub>2</sub>O to form OH radicals; these radicals are the main source of OH  
58 radicals in the troposphere, as shown by reactions R1 and R2. The strong dependence  
59 of OH concentration on j(O<sup>1</sup>D) was found in a number of field measurements (Ehhalt  
60 et al., 2000; Rohrer et al., 2014; Stone et al., 2012). In addition, the photolysis of NO<sub>2</sub>  
61 produces O<sup>3</sup>P, and then O<sup>3</sup>P reacts with O<sub>2</sub> to produce O<sub>3</sub>, as shown by reactions R3  
62 and R4, which is the only significant chemical source of ozone in the troposphere  
63 (Finlayson-Pitts et al., 2000). The photolysis frequencies of R1 and R3 are j(O<sup>1</sup>D) and  
64 j(NO<sub>2</sub>), respectively.





69 The photolysis frequencies are calculated by the following formula:

$$j = \int_{\lambda_1}^{\lambda_2} F(\lambda) \sigma(\lambda, T) \varphi(\lambda, T) d\lambda \quad (\text{E1})$$

71         $F(\lambda)$  is the actinic flux dependent on wavelength. Since the photolysis rates are  
72        proportional to the actinic flux and not all stations acquire a  $2\pi$  spectroradiometer or  
73        chemical actinometers for  $J$  measurements, several methods have been developed to  
74        determine actinic flux and photolysis frequencies from ground based measurements of  
75        irradiance (Kylling et al 2003, Kazadzis et al. 2000, 2004, Topaloglou et al. 2005,  
76        Trebs et al. 2009).  $\sigma(\lambda, T)$  is the absorption cross section of the species that absorbs in  
77        the wavelength range  $\lambda_1-\lambda_2$ .  $\phi(\lambda, T)$  is the quantum yield of the photodissociation  
78        reaction product.  $\lambda$ , and  $T$  represent wavelength, species and temperature,  
79        respectively.

The effect of aerosols on photolysis frequencies depends on the aerosol optical properties, SZA and altitude (Liao et al., 1999). The aerosol optical depth (AOD) characterizes the integral of the extinction coefficient of aerosols in the vertical direction. The light extinction of aerosols includes scattering and absorption, which have different effects on the actinic flux. Previous studies showed that scattering aerosols can enhance the actinic flux throughout the troposphere, while absorptive aerosols reduce the actinic flux throughout the boundary layer (Jacobson, 1998; Dickerson et al., 1997; Castro et al., 2001; Flynn et al., 2010). To distinguish between these two components, single scattering albedo (SSA) is defined as the ratio of the scattering coefficient to the total extinction coefficient. In areas with severe aerosol pollution, aerosols can significantly affect photolysis frequencies and ozone

91 production. Studies in Los Angeles (Jacobson, 1998), Mexico City (Castro et al., 2001;  
92 Raga et al., 2001; Li et al., 2011), São Paulo (de Miranda et al., 2005), Huston (Flynn  
93 et al., 2010), Europe (Real et al., 2011) and Russia (Pere et al., 2015) have found that  
94 aerosols reduce ozone concentration by 5-30% by attenuating photolysis frequencies.  
95 Studies in the eastern United States have shown that scattering aerosols increase  
96 ozone concentration by 5-60% by increasing the photolysis frequencies (Dickerson et  
97 al., 1997; He and Carmichael, 1999). Therefore, it is necessary to quantitatively  
98 evaluate the effect of aerosols on photolysis frequencies for a better understanding of  
99 ozone formation under highly polluted conditions.

100 Currently, the methods for quantitatively evaluating the influence of aerosols on  
101 photolysis frequencies mainly include radiative transfer model and parameterization  
102 method (Madronich et al., 1993). Radiative transfer model is based on an algorithm  
103 for calculating solar radiation and photolysis frequencies (Madronich et al., 1999).  
104 The observed data of related influential factors of the photolysis frequencies are taken  
105 as the model's input to calculate the photolysis frequencies. This method  
106 comprehensively considers the influence of aerosol optical properties on the  
107 photolysis frequencies, but it does not necessarily reflect the true quantitative  
108 relationship in the atmosphere due to complicated environmental conditions and thus  
109 the simulated results don't necessarily reproduce observed values well (Lefer et al.,  
110 2003; Shetter et al., 2003; Hofzumahaus et al., 2004). For example, the simulated  
111 slope of  $j(O^1D)$  vs AOD by Fast-JX algorithm within the CHIMERE model was  
112 significantly smaller than the observed slope, particularly for the high SZA values  
113 (Mailler et al., 2016). The parameterization method is based on the observation data  
114 taken from a certain region and is used to establish the parameterized relationship

115 between the photolysis frequencies and optical properties of aerosols (such as AOD).  
116 The method can reflect the actual atmospheric environment conditions; it also  
117 considers less influential factors and thus is easy to apply (Casasanta et al., 2011;  
118 Gerasopoulos et al., 2012). The disadvantage of this method is that the established  
119 parametric equations apply only to a specific region and cannot be extended to other  
120 regions.

121 With rapid economic development and urbanization in past decades, China's  
122 atmospheric pollution has become more and more severe, characterized by high  
123 concentrations of particulate matter and ozone. Satellite observations indicates that  
124 both the particulate matter and the ozone of eastern China are at higher levels  
125 compared with other locations in the globe (Verstraeten et al., 2015; Ma et al., 2014).  
126 Levels of pollution in the Beijing–Tianjin–Hebei are even more severe (Chang et al.,  
127 2009; Che et al., 2008; Zhang et al., 2014, Zhang et al., 2016). Therefore, it is  
128 necessary to study the effects of aerosols on photolysis frequencies and ozone  
129 production in the urban areas of China.

130 Previous model studies have shown that aerosols in China can affect ozone  
131 production by changing the photolysis frequencies. Tang et al. (2004) used a sulfur  
132 transmission–emission model (STEM) to discover that ozone concentration in  
133 northeastern China was reduced by 0.1–0.8% in the sandstorm due to the change in  
134 photolysis frequencies . Tie et al. (2005) used a global aerosol–chemical model to  
135 show that aerosols caused  $j(O^1D)$  and  $j(NO_2)$  to decrease in winter by 20%-30% and  
136 10%-30%, respectively, and in summer by 5%-20% and 1%-10%, respectively,

137 resulting in 2%-5% and 2% reductions in ozone concentration in winter and summer,  
138 respectively. Li et al. (2011) used an air quality model to estimate the changes in the  
139 photolysis frequencies caused by sulfate, nitrate, ammonium, and mineral dust  
140 aerosols in the central and eastern regions of China from June 1 to June 12, 2006. This  
141 study showed that the daily average  $j(O^1D)$  in the troposphere at the altitude of 1 km,  
142 3 km, and 10 km from the ground was reduced by 53%, 37-%, and 21%, respectively,  
143 resulting in a decrease in the ozone concentration by 5.4%, 3.8%, and 0.10% in the  
144 three layers. Lou et al (2014) found that with aerosols, annual mean photolysis  
145 frequencies ,  $j(O^1D)$ ) and  $j(NO_2)$ , were simulated to be reduced by 6-18% in polluted  
146 eastern China, leading to reductions in  $O_3$  of up to 0.5 ppbv in those regions in spring  
147 and summer by using the global chemical transport model (GEOS-Chem). However,  
148 all of these studies base their results on model simulations. Research using long-term  
149 observational data to evaluate the effects of aerosols on photolysis frequencies and  
150 ozone production in China has not yet been published.

151 Our overall goal is to quantitatively evaluate the effect of aerosols in urban  
152 Beijing on photolysis frequencies and thus on ozone production. First, the relationship  
153 between PM<sub>2.5</sub> and AOD was investigated. Second, based on long-term observations  
154 (2012-2015) of photolysis frequencies, we discussed the impact of AOD on photolysis  
155 frequencies ( $j(O^1D)$  and  $j(NO_2)$ ) in urban Beijing in detail. The relationship between  
156 photolysis frequencies and AOD is adequately compared with previous study in the  
157 Mediterranean (Casasanta et al., 2011; Gerasopoulos et al., 2012). Then, the  
158 quantitative relationship between photolysis frequencies, AOD, and SZA was  
159 acquired by the parameterization method, which could be used to quantitatively  
160 evaluate the effect of AOD on photolysis frequencies in Beijing. Finally, a  
161 photochemistry box model was used to evaluate the effect of aerosols on ozone

162 production.

163 **2. Methodology**

164 **2.1. Measurement**

165

166 From August 2012 to December 2015,  $j(O^1D)$  and  $j(NO_2)$  were measured  
167 continuously at PKUERS site. The data of the period during October 2012 to March  
168 2013 and August 2015 are missed due to instrument maintenance and other  
169 measurement campaigns. The site ( $39.99^\circ N$ ,  $116.31^\circ E$ ) is located on the sixth floor of  
170 a campus building at the Peking University, 20 km northwest of Tiananmen Square.  
171 The height from the ground is about 30 m. The sampling point is surrounded by  
172 classroom buildings. Concentration level and composition of air pollutants were  
173 thought to be similar to the downtown so as to be representative for the whole of  
174 Beijing (Wang et al., 2010; Xu et al., 2011; Zhang et al., 2012; Zhang et al., 2014).

175 The actinic flux was measured using a spectroradiometer and the photolysis  
176 frequencies were calculated from the absorption cross section and quantum yield of  
177 each species (Shetter and Müller, 1999). The spectroradiometer consisted of a single  
178 monochromator with a fixed grating (CARL ZEISS), an entrance optic with a  $2\pi$   
179 steradian (sr) solid angle quartz diffusor and a  $2048 \times 64$ -pixel photodiode array  
180 detector. The spectral measurements were performed with a wavelength resolution of  
181 2 nm, covering a wavelength range of 290-650 nm (Hofzumahaus et al., 1999). A  
182 1000 W National Institute of Standard and Technology (NIST) traceable lamp was

183 used for calibration under laboratory conditions (Bohn et al., 2008). The measured  
184 spectra were corrected for dark signal and stray light. For  $j(O^1D)$ , the quantum yields  
185 used were taken from Matsumi et al.(2002), while the ozone cross section was derived  
186 from Daumont et al. (1992) and Malicet et al. (1995). Measured temperatures were  
187 used to retrieve ozone absorption cross section and quantum yield. For  $j(NO_2)$ , the  
188 quantum yields used were taken from Bass et al. (1976) and Davenport et al. (1978),  
189 while the cross section was derived from Jones and Bayes (1973), Harker et al. (1977)  
190 and Davenport (1978). The calculated photolysis frequencies had a time resolution of  
191 10 s and an accuracy of  $\pm 10\%$  including uncertainties associated with the quartz  
192 receiver and stray-light effects (Edwards and Monks, 2003).

193 The optical properties of aerosols were measured by a CIMEL solar photometer  
194 (AERONET level 2 data collection, <http://aeronet.gsfc.nasa.gov/>) and the site selected  
195 is the Beijing-CAMS site ( $39.93^\circ N$ ,  $116.32^\circ E$ ), which is 6.4km from the PKUERS  
196 site. The CIMEL solar photometer is an automatic solar-sky scanning radiometer that  
197 uses selected spectral channels. The instrumentation, data acquisition, retrieval  
198 algorithms, and calibration procedure conform to the standards of the AERONET  
199 global network and have been described in detail by Fotiadi et al. (2006). The solar  
200 extinction measurement was performed every 3 minutes in the spectral range 340–  
201 1020 nm for the calculation of AOD at wavelengths 340, 380, 440, 500, 675, 870, 970,  
202 and 1020 nm. Under cloudless conditions, the overall uncertainty of AOD data is  $\pm$   
203 0.01 at  $\lambda > 440$  nm and  $\pm 0.02$  at shorter wavelengths. In this study, AOD at the  
204 wavelength of 380 nm was chosen for analysis. This wavelength was selected as it is

more representative of  $j(\text{NO}_2)$ . Additionally, at this wavelength we can better compare with the results of Gerasopoulos et al. (2012). The daytime clear-sky conditions were identified according to the presence of AOD data of AERONET since AOD data are unavailable under cloudy conditions. AE were also acquired from ARONET. The SSA (525nm) data were derived from a field campaign undertaken in August 2012. The absorption and scattering coefficients were measured with an Aethalometer (AE-31, Magee) and a Single Wavelength Integrating Nephelometer (Aurora-1000), respectively, with a time resolution of 1 minute. Five-minute averages of AOD, SSA, and photolysis frequencies were analyzed in this study. The total ozone column was obtained by OMI (Ozone Monitoring Instrument) for the year 2012-2015, using overpass data (<http://www.temis.nl/protocols/O3global.html>) (Henk et al., 2003). In addition, meteorological parameters such as temperature, relative humidity, and pressure were simultaneously observed at this site. Table 1 presents total  $\text{O}_3$  column, temperature, relative humidity, daytime clear-sky fraction and respective standard deviation for different seasons.

The analysis of the effects of aerosols on ozone production (Section 3.4) was based on the field campaign undertaken in August 2012. The relevant contents and methods of observation are shown in Table 2. Since the time resolution of VOCs is 1 hour, all data analyzed in Section 3.4 was processed as 1-hour average values. In this study, we focused on the effects of aerosols on photolysis frequencies and ozone production under cloudless conditions.

## 226    **2.2 Radiative Transfer Model Description**

227 We use the Tropospheric Ultraviolet and Visible (TUV) radiation model (version  
228 5.3) provided by Sasha Madronich (Madronich, 1993). In order to solve the radiative  
229 transfer equation, TUV uses the discrete-ordinates algorithm (DISORT) with 4  
230 streams and calculates the actinic flux spectra with wavelength range of 280-420 nm  
231 in 1 nm steps and resolution. Measured temperatures and ozone column were used to  
232 calculate the absorption cross sections and quantum yields. The key aerosol optical  
233 properties including AOD, SSA and AE were input into the model to test the effect of  
234 aerosols on photolysis frequencies. AE(380/550nm) is taken from AERONET and the  
235 mean value of 1.3 during June 2012 - December 2015 is used in TUV model.

236

237 **2.3 Photochemical box model**

238 The photochemical box model used in this study is based on a regional  
239 atmospheric chemical mechanism (RACM2) described by Goliff et al. (2013). The  
240 mechanism includes 17 stable inorganic compounds, 4 intermediate inorganic  
241 compounds, 55 stable organic compounds, and 43 intermediate organic compounds.  
242 Compounds not specifically treated in RACM are incorporated into species with  
243 similar functional groups. The isoprene-related mechanism used in this model is LIM  
244 mechanism proposed by Peeters et al. (2009). In this study, the observed NO<sub>2</sub>, CO,  
245 SO<sub>2</sub>, C<sub>2</sub>-C<sub>12</sub> NMHCs, HCHO, photolysis frequencies, temperature, pressure, and  
246 relative humidity were used as constraints to simulate the concentrations of reactive  
247 radicals (RO<sub>2</sub>, HO<sub>2</sub>, and OH), intermediate species, and associated reaction rate

constants. HONO wasn't measured during the period and was calculated according to  
 the concentration of NO<sub>2</sub> and the observed ratio of HONO to NO<sub>2</sub> at an urban site in  
 Beijing, which had a marked diurnal cycle, a maximum in the early morning (ratio  
 values up to ~0.05–0.08 in summer) and a decrease during daytime to values around  
 0.01–0.02 (Hendrick et al., 2014). The model was spun up for two days once it started  
 running in order to ensure that the simulation was stable. It was assumed that the  
 lifetime of simulated species removed by dry deposit was 24 hours. The lifetime  
 corresponds to the assumed deposit rate of 1.2 cm s<sup>-1</sup> and a well-mixed boundary  
 layer height of about 1 km (Lu et al., 2012). Net ozone production is equal to the  
 reaction rate between peroxy radicals (RO<sub>2</sub> and HO<sub>2</sub>) and NO minus the loss rate of  
 NO<sub>2</sub> and O<sub>3</sub> as shown in E2, E3, and E4 as derived by Mihelcic et al. (2003). The  
 ozone production rate (P(O<sub>3</sub>)), the ozone loss rate (D(O<sub>3</sub>)), and the net P(O<sub>3</sub>) were  
 calculated from the simulation results.

261

$$262 \quad P(O_3) = k_{HO_2+NO} [HO_2][NO] + \sum (k^i_{RO_2+NO} [RO_2^i][NO]) \quad (E2)$$

263

$$264 \quad D(O_3) = (\theta j(O^1D) + k_{OH+O_3}[OH] + k_{HO_2+O_3}[HO_2] + \\ \sum (k^j_{alkene+O_3} [alkene^j]))[O_3] + k_{OH+NO_2}[OH][NO_2] \quad (E3)$$

265

$$266 \quad net P(O_3) = P(O_3) - D(O_3) \quad (E4)$$

where  $\theta$  is the fraction of O<sup>1</sup>D from ozone photolysis that reacts with water vapor. i  
 and j represent the number of species of RO<sub>2</sub> and alkenes, respectively.

269

270    **3. Results and discussion**

271

272    **3.1 The correlation between PM<sub>2.5</sub> and AOD**

273        Compared with AOD, PM<sub>2.5</sub> is a more common proxy to evaluate the level of  
274        particulate matter pollution in spite that AOD is a more closely related parameter of  
275        photolysis frequencies. As a result, we attempted to analyze the quantitative  
276        relationship between PM<sub>2.5</sub> and AOD to evaluate the influence of PM<sub>2.5</sub> on AOD and  
277        thus on photolysis frequencies. The factors that affect this relationship include aerosol  
278        type, aerosol size distribution, aerosol distribution in the vertical direction, relative  
279        humidity (RH) and planetary boundary layer height (PBLH) (van Donkelaar et al.,  
280        2010). Figure 1 shows the correlation between AOD and PM<sub>2.5</sub> in four different  
281        seasons. The determination coefficient ( $r^2$ ) is 0.53, 0.58, 0.62 and 0.59 for spring  
282        (March, April and May), summer (June, July and August), autumn (September,  
283        October and November) and winter (December, January and February), respectively.  
284        Meanwhile, the correlation exhibits significant seasonal differences, having relatively  
285        smaller slope (23.56) in summer and relatively larger slope (73.76) in winter. This  
286        implies that PM<sub>2.5</sub> in summer has stronger light extinction capacity than in winter.  
287        One reason for the seasonal differences is the variation in RH among different seasons  
288        (Table 1). There is higher RH in summer (57.2% on average) than in winter (30.4%  
289        on average), leading to stronger hygroscopic growth of aerosol particles, and thus  
290        resulting in higher scattering ability of aerosol particles. According to another study in

urban Beijing, the higher the RH, the smaller the slope, and the higher the PBLH, the smaller the slope (Zheng, C. W et al., 2017). In addition, the slope was smaller for scattering-dominant aerosols than for absorbing-dominant aerosols, and smaller for coarse mode aerosols than for fine mode aerosols (Zheng, C. W et al., 2017). The slopes of the correlation between AOD (at 550nm) and PM<sub>2.5</sub> in this study in summer and winter are equal to 42.2 $\mu\text{g m}^{-3}$  and 119.2 $\mu\text{g m}^{-3}$ , respectively, close to that from Ma et al. (2016) (54.9 $\mu\text{g m}^{-3}$  and 110.5 $\mu\text{g m}^{-3}$ ) and Xin et al. (2016) (55.2  $\mu\text{g m}^{-3}$  and 93.4 $\mu\text{g m}^{-3}$ ), but smaller significantly than that from Zheng et al. (2017) (65~74 $\mu\text{g m}^{-3}$  and 143~158 $\mu\text{g m}^{-3}$ ). The differences mainly depend on the aerosol composition and size distribution at different observational sites in Beijing. Compared with other cities in North China (Tianjin, Shijiazhuang and Baoding) (Ma et al., 2016), the slope in Beijing for winter is significantly higher. Consequently, using PM<sub>2.5</sub> to estimate AOD has a large uncertainty due to multiple interference factors.

304

305

### 306   **3.2 Seasonal and diurnal variability of AOD and photolysis frequencies**

307   The diurnal cycles of AOD are shown in Figure 2. AOD displays obvious diurnal  
308   variation, with relatively high level at noon and low level at dawn and evening. The  
309   diurnal variation of PM<sub>2.5</sub> is significantly different from AOD. In addition, AOD has  
310   obvious seasonal differences, with the highest AOD in summer and the lowest AOD  
311   in winter. Conversely, PM<sub>2.5</sub> in winter (42 $\mu\text{g m}^{-3}$ ) is significantly higher than in  
312   summer (35 $\mu\text{g m}^{-3}$ ). In spite of lower PM<sub>2.5</sub> in summer, AOD in summer is higher due

313 to stronger extinction capacity of PM<sub>2.5</sub> as discussed in 3.1. Figure 3 shows the diurnal  
314 variation of the photolysis frequencies under cloudless conditions for each season.  
315 j(O<sup>1</sup>D) and j(NO<sub>2</sub>) are both highest in summer, followed by spring and autumn, and  
316 lowest in winter. This seasonal difference is mainly determined by the difference in  
317 SZA for the four seasons.

318 The observed mean daily maxima of photolysis frequencies at this site are lower  
319 than that observed in the eastern Mediterranean (Crete, Greece, 35°20'N, 25°40'E)  
320 (Gerasopoulos et al., 2012) by  $7.8 \times 10^{-6} \pm 5.5 \times 10^{-6}$  s<sup>-1</sup> and  $4.9 \times 10^{-6} \pm 1.8 \times 10^{-6}$  s<sup>-1</sup>  
321 for j(O<sup>1</sup>D), and  $1.9 \times 10^{-3} \pm 1.2 \times 10^{-3}$  s<sup>-1</sup> and  $3.3 \times 10^{-3} \pm 1.0 \times 10^{-3}$  s<sup>-1</sup> for j(NO<sub>2</sub>), in  
322 summer and winter respectively. The corresponding lower photolysis frequencies of  
323 Beijing than the eastern Mediterranean due to SZA difference is  $1.7 \times 10^{-6}$  s<sup>-1</sup> and  $3.0 \times$   
324  $10^{-6}$  s<sup>-1</sup> for j(O<sup>1</sup>D), and  $8.0 \times 10^{-5}$  s<sup>-1</sup> and  $6.6 \times 10^{-4}$  s<sup>-1</sup> for j(NO<sub>2</sub>) according to TUV  
325 model under aerosol-free conditions, which are significantly lower than observed  
326 decreased magnitudes. Additionally, we know that the temperature is lower in Beijing  
327 during the winter compared to conditions in Crete. The measured mean temperature in  
328 Beijing during winter is equal to  $0.53 \pm 4.2$  °C (Table 1). When we consider the  
329 temperature in Crete is 10 °C higher than in Beijing, the lower j(O<sup>1</sup>D) of Beijing than  
330 Crete is  $5.5 \times 10^{-7}$  s<sup>-1</sup>, which is also not able to compensate the j(O<sup>1</sup>D) gap between the  
331 two sites during winter. Taking into account the similar levels of ozone column  
332 concentration in the two sites, the large gap of photolysis frequencies in the two sites  
333 is mainly attributed to the higher AOD in Beijing ( $0.76 \pm 0.75$ ) than in the eastern  
334 Mediterranean ( $0.27 \pm 0.13$ ).

335 It can be seen from Figure 3 that the difference between winter and summer for  
336  $j(O^1D)$  is significantly larger than that for  $j(NO_2)$ , where the summer midday averages  
337 of  $j(O^1D)$  and  $j(NO_2)$  are 5 times and 2 times those of winter, respectively. There are  
338 two reasons for this phenomenon. One, compared with  $j(NO_2)$ ,  $j(O^1D)$  is more  
339 sensitive to the change in SZA and the same change in SZA results in a larger change  
340 in  $j(O^1D)$  than  $j(NO_2)$ . Two, the main influential factors of  $j(NO_2)$  under cloudless  
341 conditions are SZA and AOD, and the influence of ozone column concentration and  
342 temperature on  $j(NO_2)$  is negligible. However,  $j(O^1D)$  is affected significantly by the  
343 ozone column concentration and temperature, in addition to SZA and AOD. The  
344 higher ozone column concentration and lower temperature in winter than in summer  
345 lead to the difference in  $j(O^1D)$  further increasing (Table 1).

346

347

348 **3.3 The correlation between photolysis frequencies and AOD**

349 **3.3.1 The correlation between  $j(O^1D)$  and AOD**

350 In order to rule out the effect of SZA on photolysis frequencies, we chose SZA  
351 equal to  $30^\circ$  and  $60^\circ$  ( $\pm 1^\circ$ ) for analysis. Figure 4 presents the dependence of  $j(O^1D)$   
352 on AOD at different levels of ozone column concentration at SZA of  $30^\circ$  and  $60^\circ$  ( $\pm$   
353  $1^\circ$ ). The ozone column concentration has a classification width of 30 DU. This  
354 relatively large classification width is chosen to make sure that there are enough  
355 points to fit the relationship between  $j(O^1D)$  and AOD.  $j(O^1D)$  exhibits a clear

356 dependence on AOD, with a nonlinear negative correlation. The scatter of these points  
357 is mainly due to variations in ozone column and temperature. As AOD increased, the  
358 slope of  $j(O^1D)$ -AOD gradually decreases, indicating that the ability of aerosols to  
359 reduce  $j(O^1D)$  gradually decreases with AOD. This result differs from that found in  
360 Mediterranean, where  $j(O^1D)$  was linearly negatively correlated with AOD (Casasanta  
361 et al., 2011; Gerasopoulos., 2012). A larger variation range of AOD in Beijing (0-3)  
362 compared with Mediterranean (0-0.6) is one reason for the difference.

363 For further analysis, the observed relation between  $j(O^1D)$  and AOD was  
364 compared with TUV-simulated results. Panels a and b of Figure 5 present the  
365 comparison between observed and TUV-simulated  $j(O^1D)$  against AOD at a SZA of  
366 30° and 60° respectively and ozone column concentration of 330-360 DU. The  
367 observed  $j(O^1D)$  was at ozone column of 330-360DU and were scaled to the  
368 temperature of 298K.  $AE(380/550nm) = 1.3$ , ozone column = 345 and Temperature =  
369 298K were used in TUV model for all simulations. Mean Earth-Sun distance was used  
370 in the calculations of TUV model and measured j-values were scaled to the mean  
371 Earth-Sun distance. At low AOD level ( $< 0.8$ ), the observed slope of  $j(O^1D)$  vs AOD  
372 is significantly larger than the simulated slope at SSA of 0.95, and slightly larger than  
373 the simulated slope at SSA of 0.85. With AOD increasing, the observed slope  
374 decreases rapidly to the level smaller than the simulated slopes. The rapid change of  
375 the slope with AOD can be related to the variation of SSA at different AOD level.  
376 Figure 6 presents the relationship between SSA and AOD based on observed data in  
377 August 2012. The result suggests a significant correlation between SSA and AOD.

With the increase in AOD, SSA is elevated; meanwhile, the slope of SSA vs AOD is gradually reduced. Similar results in other regions have been obtained by Bais et al., 2005, Krotkov et al., 2005 and Kazadzis et al., 2012). SSA characterizes the ratio of the scattering extinction coefficient to the total extinction coefficient (scattering extinction coefficient plus absorptive extinction coefficient) of aerosols. The smaller the SSA, the higher the absorptive component and lower the scattering component of the aerosol, and the stronger the ability of the aerosol to reduce the actinic flux (Dickerson et al., 1997). Figure 6 indicates that aerosols in Beijing under low AOD conditions had a higher proportion of absorptive aerosol components than under high AOD conditions, and, as a result, had a stronger ability to reduce the photolysis frequencies, which contributed to the rapidly reduced slope of  $j(O^1D)$  vs AOD with AOD. However, due to absence of more SSA data of the period 2012-2015, we can't give more sufficient evidence for the dependence of SSA on AOD. For another perspective, Owing to the biomass burning and soot emission generated from heating, the fine mode heavily-absorbing aerosol percentage is higher in winter than in summer (Zheng et al., 2017; Liu et al., 2016; Zhang et al., 2013), and thus aerosols in winter have stronger ability to reduce the photolysis frequencies. High AOD levels often appeared in summer and low AOD levels occurred mostly in winter (Figure 2), another fact that may also explains the rapidly reduced slope of  $j(O^1D)$  vs AOD with AOD.

Comparing panels a and b of Figure 4, we see that at AOD smaller than 1, the slope of  $j(O^1D)$  vs AOD exhibits a significant dependence on SZA and the slope at 30°

400 of SZA is about 1.5-2.0 times larger than that at 60° of SZA. This result is similar to  
401 that of the observations made in the central Mediterranean (Casasanta et al., 2011).  
402 For the purpose of comparison with the study in the Mediterranean, the slope of  $j(O^1D)$   
403 vs AOD was calculated at AOD smaller than 0.7.

404 Table 3 presents slope, intercept and the determination coefficient ( $r^2$ ) of linear  
405 fits of correlation between  $j(O^1D)$  and AOD for each ozone column class at AOD  
406 smaller than 0.7. At SZA of 60° and O<sub>3</sub> column concentration of 300-330 DU, the  
407 respective slope of the linear regression indicates a reduction of  $j(O^1D)$  by  $4.2 \cdot 10^{-6} s^{-1}$   
408 per AOD unit. Gerasopoulos et al. (2012) reported that the observed slope in the  
409 eastern Mediterranean was equal to  $2.4 \cdot 10^{-6} s^{-1}$  at O<sub>3</sub> column of 300-320 DU.

410 Casasanta et al. (2011) reported that the observed slope in the central Mediterranean  
411 varied from  $2.7 \cdot 10^{-6} s^{-1}$  to  $3.9 \cdot 10^{-6}$  at O<sub>3</sub> column of 300-330 DU. All of these results  
412 are smaller than the value of the present study, indicating that aerosols in urban  
413 Beijing had a stronger extinction capacity on  $j(O^1D)$  than those in the Mediterranean  
414 that was influenced by both natural absorptive aerosols and anthropogenic aerosols.

415 Previous study indicated that SSA in Beijing ranged from 0.80 to 0.86 (Garland et al.,  
416 2009; Han et al., 2015b; Han et al., 2017; Tian et al., 2015). The relatively low SSA in  
417 Beijing could be an important reason for the stronger extinction capacity.

418

419

420    **3.3.2 The correlation between  $j(\text{NO}_2)$  and AOD**

421       Unlike  $j(\text{O}^1\text{D})$ ,  $j(\text{NO}_2)$  is negligibly affected by ozone column concentration and  
422       depends mainly on AOD and SZA under cloudless conditions. Figure 7 presents the  
423       dependence of  $j(\text{NO}_2)$  on AOD at different SZA levels under cloudless conditions.  
424       The cosine of SZA ( $\cos(\text{SZA})$ ) is categorized according to a width of 0.2. In the same  
425       category of  $\cos(\text{SZA})$ ,  $j(\text{NO}_2)$  displays a strong dependence on AOD. The scatter of  
426       these points is due to the relatively large classification width of SZA to a large extent.  
427       When  $\cos(\text{SZA})$  is at its maximum level (0.8-1), the correlation between  $j(\text{NO}_2)$  and  
428       AOD is close to linear. When  $\cos(\text{SZA})$  decreases, the correlation tends to be  
429       nonlinear. Similar to  $j(\text{O}^1\text{D})$ , the observed slopes of  $j(\text{NO}_2)$  vs AOD are also larger  
430       than TUV-simulated slope at SSA of 0.95 and 0.85 when AOD is smaller than 0.8,  
431       and decreased rapidly with increasing AOD (panels c and d of Figure 5). The reason  
432       for this result is the same with that for  $j(\text{O}^1\text{D})$  as explained above.

433       Table 4 presents the slope, intercept and the determination coefficient ( $r^2$ ) of  
434       linear fits of correlation between  $j(\text{NO}_2)$  and AOD for each ozone column class at  
435       AOD smaller than 0.7. The slope of  $j(\text{NO}_2)$  vs AOD also displays a significant  
436       dependence on  $\cos(\text{SZA})$ . The slope increases as  $\cos(\text{SZA})$  increases from 0 to 0.5  
437       and then decreases as  $\cos(\text{SZA})$  increases from 0.5 to 1. At SZA of  $60^\circ \pm 1$   
438       ( $\cos(\text{SZA})=0.5 \pm 0.015$ ), the respective slope of the linear regression indicates a  
439       reduction of  $j(\text{NO}_2)$  by  $3.2 \cdot 10^{-3} \text{ s}^{-1}$  per AOD unit. This result is larger than the value  
440       for non-dust aerosols ( $2.2 \cdot 10^{-3} \text{ s}^{-1}$ ) and close to the value for dust aerosols ( $3.1 \cdot 10^{-3} \text{ s}^{-1}$ )  
441       in the eastern Mediterranean reported by Gerasopoulos et al. (2012).

442

443 **3.4 The parameterization relationship between photolysis frequencies, AOD, and**

444 **SZA**

445

446 As analyzed above, the photolysis frequencies ( $j(O^1D)$  and  $j(NO_2)$ ) strongly  
447 depended on AOD and  $\cos(SZA)$  and could be fit into expression E5 using a quadratic  
448 polynomial form. The fitting parametric equations for  $j(NO_2)$  is shown in Table 5. For  
449  $j(O^1D)$ , both of O<sub>3</sub> column and temperature affect  $j(O^1D)$  significantly. Figure S1  
450 presents the dependence of  $j(O^1D)$  on ozone column at low AOD level (AOD<0.3)  
451 and SZA of (a)  $30^\circ \pm 1^\circ$  and (b)  $60^\circ \pm 1^\circ$ , respectively. Ozone column ranging from 270  
452 to 400 DU leads to  $j(O^1D)$  reducing about 50%. In order to evaluate the impact of  
453 temperature on  $j(O^1D)$ , we calculated the ratio of  $j(O^1D)$  at measured temperature to  
454  $j(O^1D)$  at temperature = 298K ( $j(O^1D)/ j(O^1D)_{T=298K}$ ) (Figure S2).  $j(O^1D)/j(O^1D)_{T=298K}$   
455 varied from 0.82 to 1.03 indicating that temperature changed  $j(O^1D)$  by no more than  
456 21%. Therefore, temperature played a minor role in changing  $j(O^1D)$  compared with  
457 ozone column. As a result, when we fitted the relationship among  $j(O^1D)$ , AOD and  
458  $\cos(SZA)$ , the effect of ozone column is considered but the effect of temperature is  
459 not considered. By fitting the relationship at different ozone classes (classification  
460 width=30DU), we found that ozone column increasing by 30DU results in  $j(O^1D)$  at a  
461 constant SZA and AOD decreasing by 18%. Therefore, the parametric equation for  
462  $j(O^1D)$  is transformed into the form E6, which reflects the influence of ozone column.

463 The parameters a<sub>1</sub>-a<sub>6</sub> correspond to ozone column range = 300-330 DU, thus we use  
464 315 DU as the weighted standard of ozone column. The fitting parameters a<sub>1</sub>-a<sub>6</sub> for  
465 j(O<sup>1</sup>D) is shown in Table 6.

466  $j(NO_2) = a_1 + a_2 AOD + a_3 \cos(SZA) + a_4 (AOD)^2 + a_5 AOD \cos(SZA) + a_6 (\cos(SZA))^2$

467 .....E5

468  $j(O^1D) = [a_1 + a_2 AOD + a_3 \cos(SZA) + a_4 (AOD)^2 + a_5 AOD \cos(SZA) + a_6 (\cos(SZA))^2]$   
 $\times [1 + (315 - O_3 \text{ column}) \times 0.006]$

469 .....E6

470 The coefficients of determination of the fitting equations are greater than 0.95 for  
471 j(NO<sub>2</sub>) and j(O<sup>1</sup>D) at a certain O<sub>3</sub> column, indicating that both of the photolysis  
472 frequencies strongly depended on AOD and cos(SZA), and the effect of other factors  
473 such as SSA and AE are integrated into the constant term in the parametric equation.

474 Since the ozone column concentration has greater influence on j(O<sup>1</sup>D) than on j(NO<sub>2</sub>),  
475 the parameters of fitting equations for j(NO<sub>2</sub>) are similar, but the parameters of fitting  
476 equations for j(O<sup>1</sup>D) have a large fluctuation at different O<sub>3</sub> column ranges (especially  
477 a<sub>1</sub> and a<sub>2</sub>). The parametric equations can be used to quantitatively evaluate the effect  
478 of AOD on photolysis frequencies in Beijing. According to the parametric equations,  
479 aerosols lead to a decrease in seasonal mean j(NO<sub>2</sub>) by 24% and 30% and a decrease  
480 in seasonal mean j(O<sup>1</sup>D) by 27% and 33% in summer and winter under clear-sky  
481 conditions, respectively, compared to an aerosol-free atmosphere. The decreasing  
482 ratio of the photolysis frequencies in winter is higher than in summer mainly due to  
483 the higher SZA in winter.

484

485       The effect of aerosols on photolysis frequencies in Beijing is compared with  
486       other studies. Real and Sartelet (2011) reported a reduction in  $j(\text{NO}_2)$  and  $j(\text{O}^1\text{D})$  of  
487       13%-14% due to aerosols by using the radiative transfer code Fast-J during summer  
488       2001 over European regions. Flynn et al (2010) reported that aerosols reduced  $j(\text{NO}_2)$   
489       by 3% in Huston during 2006 by using TUV model. Gerasopoulos et al (2012)  
490       reported that aerosols reduced  $j(\text{NO}_2)$  and  $j(\text{O}^1\text{D})$  by 5%-15% with 5-yr mean AOD at  
491       380nm equal to 0.27. All of these results are lower than the reduction ratio of this  
492       study mainly due to higher aerosol level in Beijing (4-yr mean AOD equal to  $0.76 \pm$   
493       0.75). Hodzic et al. (2007) simulated a 15–30%  $j(\text{NO}_2)$  photolysis reduction during  
494       the 2003 European summer heatwave in the case of absorbing biomass burning  
495       aerosols with AOD at 550 nm equal to 0.7-0.8 and SSA at 532 nm equal to 0.83-0.87.  
496       The result of Hodzic et al. (2007) is comparable with the reduction ratio of this study  
497       possibly due to the equivalent levels of AOD and SSA. In addition, Péré et al (2015)  
498       simulated a higher reduction (20–50%) in  $j(\text{NO}_2)$  and  $j(\text{O}^1\text{D})$  along the transport of  
499       the aerosol plume during the 2010 Russian summer wildfires episode. The higher  
500       reduction is due to the higher level of AOD (peak value of AOD at 400nm reached  
501       2-4), even though SSA is very high (0.97).

502

### 503       **3.5 The influence of AOD on ozone production**

504

505 In order to explain the effect of aerosol light extinction on ozone production, we  
506 used the data from the field observation campaign undertaken in August 2012. Ozone  
507 production depends on its precursors (NO<sub>x</sub> and VOCs), meteorological factors, and  
508 solar radiation. Solar radiation is the driving force for tropospheric photochemical  
509 reactions, in which  $j(O^1D)$  and  $j(NO_2)$  are both important for ozone production. On  
510 the one hand, the increase in  $j(NO_2)$  promotes the photolysis of NO<sub>2</sub>, thereby  
511 accelerating the formation of ozone. On the other hand, the increase in  $j(O^1D)$   
512 accelerates the photolysis of ozone. In addition, the increase in the photolysis  
513 frequencies will accelerate the photolysis of OVOC (especially formaldehyde and  
514 acetaldehyde), HONO, and H<sub>2</sub>O<sub>2</sub>, resulting in increases in OH and HO<sub>2</sub>, which will  
515 promote the reaction between OH and VOCs and thus produce more RO<sub>2</sub>. As a result,  
516 more ozone is produced by increasing the reaction rate between RO<sub>2</sub> (or HO<sub>2</sub>) and NO.  
517 However, the increase in OH and HO<sub>2</sub> also consumes ozone and NO<sub>2</sub>, which  
518 contributes to the increase in D(O<sub>3</sub>). In brief, the overall effect of changes in  
519 photolysis frequencies on sources and sinks of ozone determines the change in the net  
520 ozone production rate.

521 Ozone production (HO<sub>2</sub> + NO, RO<sub>2</sub> + NO), ozone loss (O<sup>1</sup>D + H<sub>2</sub>O, HO<sub>2</sub> + O<sub>3</sub>,  
522 O<sub>3</sub> + OH, NO<sub>2</sub> + OH, and O<sub>3</sub> + alkenes), and net ozone production rate during August  
523 2012 were calculated by using the box model. We used the observed photolysis  
524 frequencies (i.e.  $j_{obs}$ ) and the calculated photolysis frequencies by parametric  
525 equation under the condition of AOD equal to 0 (i.e.  $j_{AOD=0}$ ), were used to  
526 constrain the box model. The difference of simulated results in the two scenarios can

527 be attributed to the effect of aerosol light extinction. As a result, the presence of  
528 aerosols causes a decrease in both ozone production rate and loss rate, as is shown in  
529 Figure 8. Since the decreasing amplitude of the daytime ozone production rate is far  
530 larger than that of the daytime ozone loss rate, the mean daytime net production rate  
531 of ozone is reduced by 25%. This reduction is comparable with the results of the study  
532 in Mexico City, where aerosols caused a 20% reduction in the ozone concentrations  
533 (Castro et al., 2001). Studies in Houston and Crete have shown that aerosols cause  
534 ozone production rates to decrease by about 4% and 12%, respectively, which are  
535 lower than that found in this study (Flynn et al., 2010; Gerasopoulos et al., 2012).

536 The ratio of the observed photolysis frequencies to the photolysis frequencies at  
537 AOD equal to 0 is defined as JIF (Flynn et al., 2010). A JIF of less than 1 indicates  
538 that the aerosols cause a decrease in the photolysis frequencies. Figure 9 shows the  
539 relation between  $P(O_3)_{j\_obs}/P(O_3)_{j\_AOD=0}$  (or  $D(O_3)_{j\_obs}/D(O_3)_{j\_AOD=0}$ ) and JIF. The  
540 majority of JIF values were less than 1, with an average of 0.72, indicating that  
541 aerosols greatly attenuated photolysis frequencies due to high levels of AOD (average  
542 of 1.07) and low levels of SSA (average of 0.84) during the observation period.  
543  $P(O_3)_{j\_obs}/P(O_3)_{j\_AOD=0}$  and  $D(O_3)_{j\_obs}/D(O_3)_{j\_AOD=0}$  are both linearly positively  
544 correlated with JIF and the scatters are mostly above the 1:1 line. As can be seen from  
545 the figure 9, a 30% reduction in photolysis frequencies (JIF = 0.7) due to the presence  
546 of aerosols results in a decrease in ozone production rate and loss rate by about 26%  
547 and 15%, respectively. The decreasing amplitude in the ozone production rate is  
548 greater than the decrease in the ozone loss rate because the corresponding processes

549 of ozone production are all light-driven, but the corresponding processes of ozone loss  
550 are not all light-driven because the reaction of O<sub>3</sub> with alkenes does not depend on  
551 solar radiation. According to the simulated results, the reaction of ozone with alkenes  
552 during this campaign accounts for 17% of total ozone loss.

553 The diurnal profile of the mean ozone production and loss rate is shown in  
554 Figure 10. P(O<sub>3</sub>) peak midday in the 12:00-14:00 local hours at 31 ppb/h without  
555 aerosol impact and 23 ppb/h with aerosol impact. The maximum D(O<sub>3</sub>) also occurs  
556 between 12:00 and 14:00 at 4.2 ppb/h without aerosol impact and 3.5 ppb/h with  
557 aerosol impact. There is little difference between aerosol-impact and aerosol-free  
558 P(O<sub>3</sub>) (or D(O<sub>3</sub>)) in the hours of 6:00-11:00, but the difference in the afternoon  
559 (12:00-18:00) is large, indicating that the reduction effect of aerosol on ozone  
560 production mainly occurs during the afternoon.

561 The above analysis focuses on the effect of aerosol on the ozone production due  
562 to aerosol light extinction. However, it does not consider the close relationship  
563 between aerosol and ozone's gaseous precursors in the actual atmosphere. To explain  
564 this problem, we chose two adjacent days (small SZA effect) with obviously different  
565 AOD levels: a clean day (A day: August 21, 2012; AOD = 0.21, PM<sub>2.5</sub>=21.6  $\mu\text{g m}^{-3}$ )  
566 and a day with high aerosol pollution (B day; August 26, 2012; AOD = 3.2,  
567 PM<sub>2.5</sub>=125.0  $\mu\text{g m}^{-3}$ ) (Table 7). The difference in AOD between the two days can be  
568 taken to represent the maximum daytime gap of AOD for this month. The ozone  
569 column concentrations for these two days were 302 DU and 301 DU, respectively, of  
570 which the effect on j(O<sup>1</sup>D) is negligible. Under these conditions, the j(O<sup>1</sup>D) value at

571 noon time decreases from  $3.23 \times 10^5 \text{ s}^{-1}$  on A day to  $1.29 \times 10^5 \text{ s}^{-1}$  on B day (i.e., a 60%  
572 reduction) and the  $j(\text{NO}_2)$  value at noon time decreases from  $8.26 \times 10^{-3} \text{ s}^{-1}$  on A day  
573 to  $4.19 \times 10^{-3} \text{ s}^{-1}$  on B day (i.e., a 49.2% reduction). As shown in Table 7, B day has  
574 higher AOD and higher concentrations of gaseous pollutants. The concentrations of  
575 CO, NO<sub>2</sub>, HCHO and the OH reactivity of VOCs in B day are much higher than in A  
576 day, with the ratio of 3.6, 2.3, and 2.0, respectively. The simultaneous increases of  
577 gaseous pollutants and AOD are due to the fact that gaseous pollutants (NO<sub>x</sub>, SO<sub>2</sub>,  
578 and VOCs) emitted by major pollution sources in Beijing, including traffic and  
579 industry, have undergone the processes of gas-phase oxidation and nucleation to  
580 generate secondary particulate matter that contributes to aerosol light extinction.  
581 Previous studies have reported that secondary particulate matter has accounted for  
582 more than 60% of total particulate matter during severe smog pollution in Beijing  
583 summers (Han et al., 2015a; Guo et al., 2014). In addition, several studies have shown  
584 that secondary components in particulate matter (especially secondary organics and  
585 ammonium sulfate) have dominated the aerosol light extinction (Han et al., 2014; Han  
586 et al., 2017; Wang et al., 2015). Observations made in Beijing during the summer of  
587 2006 showed that ammonium sulfate and ammonium nitrate contributed 44.6% and  
588 22.3%, respectively, to the total extinction coefficient during a severe period of smog  
589 (Han et al., 2014); in the summer of 2014 in Beijing, ammonium sulfate, secondary  
590 organic aerosols, and ammonium nitrate contributed 30%, 22%, and 18%, respectively,  
591 to the total extinction coefficient (Han et al., 2017).

592 As shown in Figure 11, the simulation results indicate that the net P(O<sub>3</sub>) of B day

593 is 36.2% higher than that of A day due to higher concentrations of ozone precursors  
594 on B day. This result is consistent with the observed ozone concentrations, of which  
595 the observed ozone concentration in B day is 2.2 times higher than that of A day. If we  
596 adjust the photolysis frequencies level of B day to the level of A day, the net  $P(O_3)$   
597 increases by 70.0%, which indicates that the high level of particulate matter in B day  
598 greatly inhibits ozone production. This result means that the system is under negative  
599 feedback, thus keeping  $O_3$  at a relatively stable level. Table 8 summarizes the average  
600 levels of gaseous pollutants and photolysis frequencies for AOD less than 1 and  
601 greater than 1, as measured during August 2012. It shows that, the concentrations of  
602 ozone's precursors are higher and the photolysis frequencies are lower at high AOD  
603 levels ( $AOD > 1$ ) than those at low AOD level ( $AOD < 1$ ). This result means that the  
604 negative feedback mechanism is prevalent throughout the whole campaign period.  
605 Therefore, the prevention and control measures of air pollution in Beijing need to  
606 incorporate this coupling mechanism between particulate matter and ozone to achieve  
607 effective control of these two main pollutants.

608 **4. Conclusion**

609 Photolysis reactions are important driving forces for tropospheric photochemical  
610 oxidation processes and ozone production. In this study, we explored in detail the  
611 effects of aerosols on photolysis frequencies and ozone production in Beijing, based  
612 on a long observation period of 4 years. We have found that:

- 613 (1) There is a strong correlation between PM<sub>2.5</sub> and AOD, and the slope in  
614 summer is smaller significantly than in winter, which indicates that aerosols  
615 in summer have a more efficient extinction capacity than in winter.
- 616 (2) As AOD increased, the extinction effect of aerosol on photolysis frequencies  
617 was decreased; this result was probably related to a higher proportion of  
618 scattering aerosols under high AOD conditions than under low AOD  
619 conditions. The slope of the correlation between photolysis frequencies and  
620 AOD indicates that the aerosols in urban Beijing have a stronger extinction  
621 on actinic flux than absorptive dust aerosols in the Mediterranean.
- 622 (3) The influence of AOD on photolysis frequencies was evaluated quantitatively  
623 by establishing parametric equations. According to the parametric equation,  
624 aerosols lead to a decrease in seasonal mean  $j(\text{NO}_2)$  by 24% and 30% for  
625 summer and winter, respectively, and the corresponding decrease in seasonal  
626 mean  $j(\text{O}^1\text{D})$  by 27% and 33% respectively, compared to an aerosol-free  
627 atmosphere.
- 628 (4) In order to evaluate the effects of aerosols on ozone production rate, we  
629 carried out an observation campaign in August 2012. The results show that  
630 aerosols reduced the net ozone production rate by 25% by reducing the  
631 photolysis frequencies. High concentrations of ozone gaseous precursors  
632 were often accompanied by high concentrations of particulate matter, which,  
633 to a large extent, inhibited excessive levels of ozone generation and reflected  
634 the negative feedback effect of the atmospheric system. Therefore, the

635 influence of aerosol on photolysis frequencies and thus on the rate of  
636 oxidation of VOCs and NO<sub>x</sub> to ozone and secondary aerosol is important for  
637 determining the atmospheric effects of controlling the precursor emissions of  
638 these two important air pollutants (aerosols and ozone).

639

640 **Author contribution**

641

| Author      | Contribution   |
|-------------|--|
| Wenjie Wang | acquisition of data; analysis and interpretation of data;<br>drafting the article and revising it critically |
| Min Shao    | substantial contributions to conception and design; revising<br>the article critically                       |
| Min Hu      | collection of data   |
| Limin Zeng  | collection of data   |
| Yusheng Wu  | collection of data   |

642

643

644

645

646

647 **ACKNOWLEDGEMENTS**

648 This work was supported by the Major Program of the National Natural Science  
649 Foundation of China [Grant number 91644222]. We thank Hongbin Chen and Philippe  
650 Goloub for data management of AOD and other aerosol optical properties on  
651 AERONET.

652      **Reference**

- 653      Barnarda, J. C., Chapman E G., Fasta, J. D., Schmelzera, J. R., Slusserb, J. R.,  
654      Shetterc, R. E.: An evaluation of the FAST-Jphotolysis algorithm for predicting  
655      nitrogen dioxide photolysis rates under clear and cloudy sky conditions,  
656      ATMOSPHERIC ENVIRONMENT, 38, 3393-3403,  
657      10.1016/j.atmosenv.2004.03.034, 2004.
- 658      Bais, A. F., Kazantidis, A., Kazadzis, S., Balis, D. S., Zerefos, C. S., Meleti, C.  
659      Deriving an effective aerosol single scattering albedo from spectral surface UV  
660      irradiance measurements, ATMOSPHERIC ENVIRONMENT, 39, 1093-1102,  
661      DOI: 10.1016/j.atmosenv.2004.09.080, 2005.
- 662      Bass, A. M., Ledford, A, E., and Laufer, A. H., Extinction coefficients of NO<sub>2</sub> and  
663      N<sub>2</sub>O<sub>4</sub>, J. Res. Nat. Bureau Standards, 80A, 143-162, 1976.
- 664      Bohn, B., Corlett, G. K., Gillmann, M., Sanghavi, S., Stange, G., Tensing, E.,  
665      Vrekoussis, M., Bloss, W. J., Clapp, L. J., Kortner, M., Dorn, H. P., Monks, P. S.,  
666      Platt, U., Plass-Dulmer, C., Mihalopoulos, N., Heard, D. E., Clemithshaw, K. C .,  
667      Meixner, F. X., Prevot, A. S. H., Schmitt, R.: Photolysis frequency measurement  
668      techniques: Results of a comparison within the ACCENT project,  
669      ATMOSPHERIC CHEMISTRY AND PHYSICS, 8, 5373–5391,  
670      doi:10.5194/acp-8-5373-2008, 2008.
- 671      Casasanta, G., di Sarra, A., Meloni, D., Monteleone, F., Pace, G., Piacentino, S.,  
672      Sferlazzo, D.: Large aerosol effects on ozone photolysis in the Mediterranean,  
673      ATMOSPHERIC ENVIRONMENT, 45, 3937-3943,  
674      10.1016/j.atmosenv.2011.04.065, 2011.
- 675      Castro, T., Madronich, S., Rivale, S., Muhlia, A., Mar, B.: The influence of aerosols  
676      on photochemical smog in Mexico City, ATMOSPHERIC ENVIRONMENT, 35,  
677      1765-1772, 10.1016/S1352-2310(00)00449-0, 2001.
- 678      Chang, D, Song, Y, Liu, B.: Visibility trends in six megacities in China 1973–2007,  
679      ATMOSPHERIC RESEARCH, 94, 161-167, 10.1016/j.atmosres.2009.05.006,

- 680           2009.
- 681       Che, H., Zhang, X., Li, Y., Zhou, Z., Qu, J. J., Hao, X.: Haze trends over the capital  
682       cities of 31 provinces in China, 1981–2005, THEORETICAL AND APPLIED  
683       CLIMATOLOGY, 97, 235-242, 10.1007/s00704-008-0059-8, 2009.
- 684       de Miranda, R., Andrade, M. F., Fattori, A. P.: Preliminary studies of the effect of  
685       aerosols on nitrogen dioxide photolysis rates in the city of Sao Paulo, Brazil.  
686       ATMOSPHERIC RESEARCH, 75, 135–148, 10.1016/j.atmosres.2004.12.004,  
687       2005.
- 688       Daumont, D., Brion, J., Charbonnier, J., Malicet, J. Ozone UV spectroscopy I:  
689       absorption cross-sections at room temperature. Journal of Atmospheric  
690       Chemistry 15, 145-155, 1992.
- 691       Davenport, J.E. Determination of NO<sub>2</sub> photolysis parameters for stratospheric  
692       modelling, FAA Report No. FAA-EQ-7-14, 1978.
- 693       Dickerson, R. R., Kondragunta, S., Stenchikov, G., Civerolo, K. L., Doddridge, B. G.,  
694       Holben, N.: The impact of aerosols on solar ultraviolet radiation and  
695       photochemical smog, Science, 278, 827–830, 10.1126/science.278.5339.827,  
696       1997.
- 697       Ehhalt, D. H., Rohrer, F.: Dependence of the OH concentration on solar UV,  
698       JOURNAL OF GEOPHYSICAL RESEARCH-ATMOSPHERES, 105,  
699       3565-3571, 10.1029/1999JD901070, 2000.
- 700       Eskes, H. J., Van Velthoven, P. F. J., Valks, P. J. M., Kelder, H. M. Assimilation of  
701       GOME total ozone satellite observations in a three-dimensional tracer transport  
702       model, Q.J.R.Meteorol.Soc. 129, 1663-1681, [doi:10.1256/qj.02.14](https://doi.org/10.1256/qj.02.14), 2003.
- 703       Finlayson-Pitts, B. J., Pitts, J. N.: Chemistry of the Upper and Lower Atmosphere.  
704       Academic Press, New York, 2000.
- 705       Flynn, J., Lefer, B., Rappenglück, B., Leuchner, M., Perna, R., Dibb, J., Ziembka, L.,  
706       Anderson, C., Stutz, J., Brune, W., Ren, X. R.: Impact of clouds and aerosols on  
707       ozone production in Southeast Texas. ATMOSPHERIC ENVIRONMENT, 44,  
708       4126–4133, 10.1016/j.atmosenv.2009.09.005, 2010.

- 709 Fotiadi, A., Hatzianastassiou, N., Drakakis, E., Matsoukas, C., Pavlakis, K. G.,  
710 Hatzidimitriou, D., Gerasopoulos, E., Mihalopoulos, N., Vardavas, I.: Aerosol  
711 physical and optical properties in the eastern Mediterranean Basin, Crete, from  
712 Aerosol Robotic Network data, ATMOSPHERIC CHEMISTRY AND PHYSICS,  
713 6, 5399–5413, 10.5194/acp-6-5399-2006, 2006
- 714 Gao W, Tie X X, Xu J M, Huang R J, Mao X Q, Zhou G Q, Luyu Chang. Long-term  
715 trend of O<sub>3</sub> in a mega City (Shanghai), China: Characteristics, causes, and  
716 interactions with precursors. SCIENCE OF THE TOTAL ENVIRONMENT, 603,  
717 425–433, 10.1016/j.scitotenv.2017.06.099, 2017.
- 718 Garland, R.; O. Schmid, A.; Nowak, P.; Achtert, A.; Wiedensohler, S.; Gunthe, N.;  
719 Takegawa, K.; Kita, Y.; Kondo, and M. Hu (2009), Aerosol optical properties  
720 observed during Campaign of Air Quality Research in Beijing 2006  
721 (CAREBeijing-2006): Characteristic differences between the inflow and outflow  
722 of Beijing city air, JOURNAL OF GEOPHYSICAL  
723 RESEARCH-ATMOSPHERES, 114, D00G04, 10.1029/2008JD010780, 2009.
- 724 Gerasopoulos, E., Kazadzis, S., Vrekoussis, M., Kouvarakis, G., Liakakou, E.,  
725 Kouremeti, N., Giannadaki, D., Kanakidou, M., Bohn, B., Mihalopoulos, N.:  
726 Factors affecting O<sub>3</sub> and NO<sub>2</sub> photolysis frequencies measured in the eastern  
727 Mediterranean during the five-year period 2002–2006, JOURNAL OF  
728 GEOPHYSICAL RESEARCH-ATMOSPHERES, 117, D22305,  
729 10.1029/2012JD017622, 2012.
- 730 Goliff, W. S., Stockwell, W. R., Lawson, C. V.: The regional atmospheric chemistry  
731 mechanism, version 2, ATMOSPHERIC ENVIRONMENT, 68, 174–185,  
732 10.1016/j.atmosenv.2012.11.038, 2013.
- 733 Guo, S., Hu M, Zamora, M. L., Peng, J. F., Shang, D. J., Zheng, J., Du, Z. F., Wu, Z.  
734 J., Shao, M., Zeng, L. M., Molina, M. J., Zhang, R. Y.: Elucidating severe urban  
735 haze formation in China, PROCEEDINGS OF THE NATIONAL ACADEMY  
736 OF SCIENCES OF THE UNITED STATES OF AMERICA, 111, 17373–17378,  
737 10.1073/pnas.1419604111, 2014.

- 738 Han, T. T., Liu, X. G., Zhang, Y. H., Qu, Y., Gu, J. W., Ma, Q., Lu, K. D., Tian, H. Z.,  
739 Chen, J., Zeng, L. M.: Characteristics of aerosol optical properties and their  
740 chemical apportionments during CAREBeijing 2006, AEROSOL AND AIR  
741 QUALITY RESEARCH, 14: 1431-1442, 10.4209/aaqr.2013.06.0203, 2014.
- 742 Han, T. T., Xu, W. Q., Chen, C., Liu, X. G., Wang, Q. Q., Li, J., Zhao, X. J., Du, W.,  
743 Wang, Z. F., Sun, Y. L.: Chemical apportionment of aerosol optical properties  
744 during the Asia-Pacific Economic Cooperation summit in Beijing, China,  
745 JOURNAL OF GEOPHYSICAL RESEARCH-ATMOSPHERES, 120,  
746 10.1002/2015JD023918, 2015b.
- 747 Han, T. T., Xu, W. Q., Li, J., Freedman, A., Zhao, J., Wang, Q. Q., Chen, C., Zhang, Y.  
748 J., Wang, Z. F., Fu, P. Q.: Aerosol optical properties measurements by a CAPS  
749 single scattering albedo monitor: Comparisons between summer and winter in  
750 Beijing, China, JOURNAL OF GEOPHYSICAL RESEARCH-ATMOSPHERES,  
751 122, 2513-2526, 10.1002/2016JD025762, 2017.
- 752 Han, T., Liu, X., Zhang, Y., Qu, Y., Zeng, L., Hu, M., Zhu, T.: Role of secondary  
753 aerosols in haze formation in summer in the Megacity Beijing, JOURNAL OF  
754 ENVIRONMENTAL SCIENCES, 31, 51-60, 10.1016/j.jes.2014.08.026, 2015a.
- 755 Harker, A. B., Ho, W., and Ratto, J. J. Photodissociation quantum yields of NO<sub>2</sub> in the  
756 region 375 to 420 nm, Chem Phys. Lett. 50, 394-397, 1977.
- 757 He, S., Carmichael, G. R.: Sensitivity of photolysis rates and ozone production in the  
758 troposphere to aerosol properties, JOURNAL OF GEOPHYSICAL  
759 RESEARCH-ATMOSPHERES, 104, 26307–26324, 10.1029/1999JD900789,  
760 1999.
- 761 Hendrick, F; Muller, JF; Clemer, K; Wang, P; De Maziere, M; Fayt, C; Gielen, C;  
762 Hermans, C; Ma, JZ; Pinardi, G ; Stavrakou, T; Vlemmix, T; Van Roozendael,  
763 M., Four years of ground-based MAX-DOAS observations of HONO and NO<sub>2</sub> in  
764 the Beijing area. ATMOSPHERIC CHEMISTRY AND PHYSICS, 14(2),  
765 765-781, 2014. Hodzic, A., Madronich, S., Bohn, B., Massie, S., Menut, L., and  
766 Wiedinmyer, C.: Wildfire particulate matter in Europe during summer 2003:

- 767 meso-scale modeling of smoke emissions, trans-port and radiative effects,  
768 ATMOSPHERIC CHEMISTRY AND PHYSICS, 7, 4043–4064,  
769 10.5194/acp-7-4043-2007, 2007.
- 770 Hofzumahaus, A., Kraus, A., Muller, M.: Solar actinic flux spectroradiometry: A  
771 technique for measuring photolysis frequencies in the atmosphere, APPLIED  
772 OPTICS, 38, 4443–4460, 10.1364/AO.38.004443, 1999.
- 773 Hofzumahaus, A., Lefer, B. L., Monks, P. S., Hall, S. R., Kylling, A., Mayer, B.,  
774 Shetter, R. E., Junkermann, W., Bais, A., Calvert, J. G., Cantrell, C. A.,  
775 Madronich, S., Edwards, G. D., Kraus, A.: Photolysis frequency of O<sub>3</sub> to O(<sup>1</sup>D):  
776 Measurements and modeling during the International Photolysis Frequency  
777 Measurement and Modeling Intercomparison (IPMMI), JOURNAL OF  
778 GEOPHYSICAL RESEARCH-ATMOSPHERES, 109 (D8), D08S90,  
779 10.1029/2003JD004333, 2004.
- 780 Jacobson, M, Z.: Studying the effects of aerosols on vertical photolysis rate  
781 coefficient and temperature profiles over an urban airshed, JOURNAL OF  
782 GEOPHYSICAL RESEARCH-ATMOSPHERES, 103, 10593–10604,  
783 10.1029/98JD00287, 1998.
- 784 Jones, I. T. N. and Bayes, K.D. Photolysis of nitrogen dioxide, J. Chem. Phys. 59,  
785 4836-4844, 1973.
- 786 Kazadzis, S., Bais, A. F., Balis, D., Zerefos, C. S., and Blumthaler, M. Retrieval of  
787 down-welling UV actinic flux density spectra from spectral measurements of  
788 global and direct solar UV irradiance, J. Geophys. Res., 105, 4857-4864, 2000.
- 789 Kazadzis, S., Topaloglou, C., Bais, A. F., Blumthaler, M., Balis, D., Kazantzidis, A.,  
790 Schallhart, B. Actinic flux and O<sup>1</sup>D photolysis frequencies retrieved from  
791 spectral measurements of irradiance at Thessaloniki, Greece, ATMOSPHERIC  
792 CHEMISTRY AND PHYSICS, 4, 2215-2226, DOI: 10.5194/acp-4-2215-2004,  
793 2004.
- 794 Kazadzis, S., Amiridis, V., and Kouremeti, N. The Effect of Aerosol Absorption in  
795 Solar UV Radiation, Advances in Meteorology, Climatology and Atmospheric

- 796 Physics, 1041-1047, 2012.
- 797 Krotkov, N., Bhartia, P. K., Herman, J., Slusser, J., Scott, G., Labow, G., Vasilkov, A.  
798 P., Eck, T. F., Dubovik, O., Holben, B. N. Aerosol ultraviolet absorption  
799 experiment (2000 to 2004), part 2: Absorption optical thickness, refractive index,  
800 and single scattering albedo, OPTICAL ENGINEERING, 44, 4, 041005. DOI:  
801 10.1117/1.1886819, 2005.
- 802 Kylling, A., Webb, A. R., Bais, A. F., Blumthaler, M., Schmitt, R., Thiel, S.,  
803 Kazantzidis, A., Kift, R., Misslebeck, M., Schallhart, B., Schreder, J., Topaloglou,  
804 C., Kazadzis, S., and Rimmer, J.: Actinic flux determination from measurements  
805 of irradiance, J. Geophys. Res., 108 (D16), 4506-4515, 2003.
- 806 Lefer, B. L., Shetter, R. E., Hall, S. R.: Impact of clouds and aerosols on photolysis  
807 frequencies and photochemistry during TRACE-P: 1. Analysis using radiative  
808 transfer and photochemical box models, JOURNAL OF GEOPHYSICAL  
809 RESEARCH-ATMOSPHERES, 108, 8821-8835, 10.1029/2002JD003171, 2003.
- 810 Li C C, Mao J T, Liu Q H. Using MODIS to study the distribution and seasonal  
811 variation of aerosol optical thickness in eastern China. Science Bulletin (China),  
812 48: 2094-2100. 2003.
- 813 Li, J., Wang, Z. F., Wang, X., Yamaji, K., Takigawa, M., Kanaya, Y., Pochanart, P.,  
814 Liu, Y., Irie, H., Hu, B., Tanimoto, H., Akimoto, H.: Impacts of aerosols on  
815 summertime tropospheric photolysis frequencies and photochemistry over  
816 Central Eastern China, ATMOSPHERIC ENVIRONMENT, 45: 1817-1829,  
817 10.1016/j.atmosenv.2011.01.016, 2011.
- 818 Liao, H., Yung, Y. L., and Seinfeld, J. H.: Effects of aerosols on tropospheric  
819 photolysis rates in clear and cloudy atmospheres, JOURNAL OF  
820 GEOPHYSICAL RESEARCH, 104(D19), 23697–23707, 1999.
- 821 Liu, Q.Y., Ma, T. M., Olson, M. R., Liu, Y. J., Zhang, T. T., Wu, Y., Schauer, J. J.:  
822 Temporal variations of black carbon during haze and non-haze days in Beijing,  
823 SCIENTIFIC REPORTS, 6, 33331, 10.1038/srep33331, 2016.

- 824 Lou, S. J; Liao, H; Zhu, B. Impacts of aerosols on surface-layer ozone concentrations  
825 in China through heterogeneous reactions and changes in photolysis rates.  
826 ATMOSPHERIC ENVIRONMENT, 85:123-138,  
827 0.1016/j.atmosenv.2013.12.004, 2014.
- 828 Lu, K. D., Rohrer, F., Holland, F., Fuchs, H., Bohn, B., Brauers, T., Chang, C. C.,  
829 Häseler, R., Hu, M., Kita, K., Kondo, Y., Li, X., Lou, S. R., Nehr, S., Shao, M.,  
830 Zeng, L. M., Wahner, A., Zhang, Y. H., Hofzumahaus, A.: Observation and  
831 modelling of OH and HO<sub>2</sub> concentrations in the Pearl River Delta 2006: a  
832 missing OH source in a VOC rich atmosphere, ATMOSPHERIC CHEMISTRY  
833 AND PHYSICS, 12: 1541-1569, 10.5194/acp-12-1541-2012, 2012
- 834 Ma, X. Y., Wang, J. Y., Yu, F. Q., Jia, H. L., Hu, Y. N.: Can MODIS AOD be  
835 employed to derive PM<sub>2.5</sub> in Beijing-Tianjin-Hebei over China?  
836 ATMOSPHERIC RESEARCH, 181, 250-256, 10.1016/j.atmosres.2016.06.018,  
837 2016.
- 838 Ma, Z. W., Hu, X. F., Huang, L., Bi, J., Liu, Y.: Estimating Ground-Level PM<sub>2.5</sub> in  
839 China Using Satellite Remote Sensing. Environ Sci Technol, 48: 7436–7444.
- 840 Madronich, S, The Atmosphere and UV-B Radiation at Ground Level, Environmental  
841 UV Photobiology, doi: 0.1007/978-1-4899-2406-3\_1. 1993,
- 842 Madronich, S., and S. Flocke, The role of solar radiation in atmospheric chemistry, in  
843 Environmental Photochemistry, edited by P. Boule, pp. 1-26, Springer-Verlag,  
844 New York, 1999.
- 845 Mailler, S., Menut, L., di Sarra, A. G., Becagli, S., Di Iorio, T., Bessagnet, B., Briant,  
846 R., Formenti, P., Doussin, J. F ., Gomez-Amo, J. L., Mallet, M., Rea, G., Siour, G.,  
847 Sferlazzo, D. M., Traversi, R., Udisti, R., Turquety, S.: On the radiative impact of  
848 aerosols on photolysis rates: comparison of simulations and observations in the  
849 Lampedusa island during the ChArMEx/ADRIMED campaign, ATMOSPHERIC  
850 CHEMISTRY AND PHYSICS, 16(3):1219-1244, 10.5194/acp-16-1219-2016,  
851 10.5194/acp-16-1219-2016, 2016.
- 852 Matsumi, Y., Comes, F.J., Hancock, G., Hofzumahaus, A., Hynes, A.J., Kawasaki, M.,

- 853 Ravishankara, A.R., Quantum yields for production of O(<sup>1</sup>D) in the ultraviolet  
854 photolysis of ozone: recommendation based on evaluation of laboratory data.  
855 Journal of Geophysical Research 107 (D3), 4024. doi:10.1029/2001JD000510.  
856 2002.
- 857 Malicet, J., Daumont, D., Charbonnier, J., Parisse, C., Chakir, A., Brion, J. Ozone UV  
858 spectroscopy. II. Absorption cross-sections and temperature dependence. Journal  
859 of Atmospheric Chemistry 21 (3), 263-273, 1995.
- 860 Peeters, J., Nguyen, T. L., Vereecken, L.: HOX radical regeneration in the oxidation of  
861 isoprene. PHYSICAL CHEMISTRY CHEMICAL PHYSICS, 11: 5935-5939,  
862 10.1039/b908511d, 2009.
- 863 Pere, J. C., Bessagnet, B., Pont, V., Mallet, M., Minvielle, F.: Influence of the aerosol  
864 solar extinction on photochemistry during the 2010 Russian wildfires episode,  
865 ATMOSPHERIC CHEMISTRY AND PHYSICS, 15, 10983-10998,  
866 10.5194/acp-15-10983-2015, 2015.
- 867 Raga, G. B., Castro, T., Baumgardner, D.: The impact of megacity pollution on local  
868 climate and implications for the regional environment: Mexico City,  
869 ATMOSPHERIC ENVIRONMENT, 35, 1805-1811,  
870 10.1016/S1352-2310(00)00275-2, 2001.
- 871 Real, E. and Sartelet, K.: Modeling of photolysis rates over Europe: impact on  
872 chemical gaseous species and aerosols, ATMOSPHERIC CHEMISTRY AND  
873 PHYSICS, 11, 1711–1727, 10.5194/acp-11-1711-2011, 2011.
- 874 Rohrer, F; Lu, K. D; Hofzumahaus, A; Bohn, B ; Brauers, T ; Chang, C. C ; Fuchs, H;  
875 Haseler, R; Holland, F; Hu, M., Maximum efficiency in the  
876 hydroxyl-radical-based self-cleansing of the troposphere, Nature Geoscience. 7,  
877 559-563, 2014.
- 878 Shetter, R. E., Muller, M.: Photolysis frequency measurements using actinic flux  
879 spectroradiometry during PEM-Tropics Mission: Instrumentation description and  
880 some results, JOURNAL OF GEOPHYSICAL RESEARCH-ATMOSPHERES,  
881 104, 5647-5661, 10.1029/98JD01381, 1999.

- 882 Shetter, R. E.: Photolysis frequency of NO<sub>2</sub>: measurement and modeling during the  
883 International Photolysis Frequency Measurement and Modeling Intercomparison  
884 (IPMMI), JOURNAL OF GEOPHYSICAL RESEARCH-ATMOSPHERES, 108,  
885 8544, 10.1029/2002JD002932, 2003.
- 886 Stone, D; Whalley, L. K; Heard, D. E. Tropospheric OH and HO<sub>2</sub> radicals: field  
887 measurements and model comparisons, Chem. Soc. Rev.,41(19): 6348-6404,  
888 10.1039/c2cs35140d, 2012.
- 889 Tang, Y., Carmichael, G. R., Kurata, G., Uno, I., Weber, R. J., Song, C. H., Guttikunda,  
890 S. K., Woo, J. H., Streets, D. G., Wei, C., Clarke, A. D., Huebert, B., Anderson, T.  
891 L.: Impacts of dust on regional tropospheric chemistry during the ACE-Asia  
892 experiment: a model study with observations, JOURNAL OF GEOPHYSICAL  
893 RESEARCH-ATMOSPHERES, 109, D19S21, 10.1029/2003JD003806, 2004.
- 894 Tian, P., Wang, G. F., Zhang, R. J., Wu, Y. F., Yan, P.: Impacts of aerosol chemical  
895 compositions on optical properties in urban Beijing, China, PARTICUOLOGY,  
896 18, 155-164, 10.1016/j.partic.2014.03.014, 2015.
- 897 Tie, X. X., Madronich, S., Walters, S., Edwards, D. P., Ginoux, P., Mahowald, N.,  
898 Zhang, R. Y., Lou, C., Brasseur, G.: Assessment of the global impact of aerosols  
899 on tropospheric oxidants. JOURNAL OF GEOPHYSICAL  
900 RESEARCH-ATMOSPHERES, 110, D03204, 10.1029/2004JD005359, 2005.
- 901 Topaloglou, C., Kazadzis, S., Bais, AF., Blumthaler, M., Schallhart, B., Balis, D. NO<sub>2</sub>  
902 and HCHO photolysis frequencies from irradiance measurements in Thessaloniki,  
903 Greece. ATMOSPHERIC CHEMISTRY AND PHYSICS, 5, 1645-1653, DOI:  
904 10.5194/acp-5-1645-2005, 2005.
- 905 Trebs, I., Bohn, B., Ammann, C., Rummel, U., Blumthaler, M., Konigstedt, R.,  
906 Meixner, F. X ., Fan, S., Andreae, M. O. Relationship between the NO<sub>2</sub> photolysis  
907 frequency and the solar global irradiance, ATMOSPHERIC MEASUREMENT  
908 TECHNIQUES, 2, 725-739, DOI: 10.5194/amt-2-725-2009, 2009. van Donkelaar,  
909 A., Martin, R. V., Brauer, M., Kahn, R., Levy, R., Verduzco, C., and Villeneuve,  
910 P. J.: Global Estimates of Ambient Fine Particulate Matter Concentrations from

- 911 Satellite-Based Aerosol Optical Depth: Development and Application.  
912 Environmental Health Perspectives, 118, 847-855, 10.1289/ehp.0901623, 2010.
- 913 van Donkelaar, A., Martin, R. V., Brauer, M., Kahn, R., Levy, R., Verduzco, C., and  
914 Villeneuve, P. J.: Global Estimates of Ambient Fine Particulate Matter  
915 Concentrations from Satellite-Based Aerosol Optical Depth: Development and  
916 Application. Environmental Health Perspectives, 118, 847-855,  
917 10.1289/ehp.0901623, 2010.
- 918 Verstraeten, W. W., Neu, J. L., Williams, J. E., Bowman, K. W., Worden, J. R.,  
919 Boersma, K. F.: Rapid increases in tropospheric ozone production and export  
920 from China. NATURE GEOSCIENCE, 8, 690-695, 10.1038/NGEO2493, 2015.
- 921 Volkamer R, Sheehy P, Molina L T, Molina M J.: Oxidative capacity of the Mexico  
922 City atmosphere – Part 1: A radical source perspective, ATMOSPHERIC  
923 CHEMISTRY AND PHYSICS, 10, 6969–6991, 10.5194/acp-10-6969-2010,  
924 2010.
- 925 Wang, B., Shao, M., Lu, S. H., Yuan, B., Zhao, Y., Wang, M., Zhang, S. Q., Wu, D.:  
926 Variation of ambient non-methane hydrocarbons in Beijing city in summer 2008,  
927 ATMOSPHERIC CHEMISTRY AND PHYSICS, 10, 5911–5923,  
928 10.5194/acp-10-5911-2010, 2010.
- 929 Wang, Q., Sun, Y., Jiang, Q., Du, W., Sun, C., Fu, P., Wang, Z.: Chemical  
930 composition of aerosol particles and light extinction apportionment before and  
931 during the heating season in Beijing, China. JOURNAL OF GEOPHYSICAL  
932 RESEARCH-ATMOSPHERES, 120: 12,708-12,722, 10.1002/2015JD023871,  
933 2015.
- 934 Xin, J. Y; Gong, C. S; Liu, Z. R; Cong, Z. Y; Gao, W. K; Song, T; Pan, Y. P; Sun, Y;  
935 Ji, D. S; Wang, L. L; Tang, G. Q; Wang, Y. S.: The observation-based  
936 relationships between PM<sub>2.5</sub> and AOD over China, JOURNAL OF  
937 GEOPHYSICAL RESEARCH-ATMOSPHERES, 121, 10701-10716,  
938 10.1002/2015JD024655, 2016.

- 939 Xu, J., Ma, J. Z., Zhang, X. L., Xu, X. B., Xu, X. F., Lin, W. L., Wang, Y., Meng, W.,  
940 and Ma, Z. Q.: Measurements of ozone and its precursors in Beijing during  
941 summertime: impact of urban plumes on ozone pollution in downwind rural  
942 areas, ATMOSPHERIC CHEMISTRY AND PHYSICS, 11, 12241–12252,  
943 10.5194/acp-11-12241-2011, 2011.
- 944 Zhang, J. P., Zhu, T., Zhang, Q. H., Li, C. C., Shu, H. L., Ying, Y., Dai, Z. P., Wang, X.,  
945 Liu, X. Y., Liang, A. M., Shen, H. X., and Yi, B. Q.: The impact of circulation  
946 patterns on regional transport pathways and air quality over Beijing and its  
947 surroundings, ATMOSPHERIC CHEMISTRY AND PHYSICS, 12, 5031–5053,  
948 10.5194/acp-12-5031-2012, 2012.
- 949 Zhang, L.; Shao, J.; Lu, X.; Zhao, Y.; Hu, Y.; Henze, D. K.; Liao, H.; Gong, S.; Zhang,  
950 Q.: Sources and Processes Affecting Fine Particulate Matter Pollution over North  
951 China: An Adjoint Analysis of the Beijing APEC Period. ENVIRONMENTAL  
952 SCIENCE & TECHNOLOGY, 50(16), 8731-8740, 10.1021/acs.est.6b03010,  
953 2016.
- 954 Zhang, Q., Yuan, B., Shao, M., Wang, X., Lu, S., Lu, K., Wang, M., Chen, L., Chang,  
955 C. C., Liu, S. C.: Variations of ground-level O<sub>3</sub> and its precursors in Beijing in  
956 summertime between 2005 and 2011, ATMOSPHERIC CHEMISTRY AND  
957 PHYSICS, 14, 6089-6101, 10.5194/acp-14-6089-2014, 2014.
- 958 Zhang, R., Jing, J., Tao, J., Hsu, S. C., Wang, G., Cao, J., Lee, C. S. L., Zhu, L., Chen,  
959 Z., Zhao, Y., Shen, Z.: Chemical characterization and source apportionment of  
960 PM<sub>2.5</sub> in Beijing: seasonal perspective, ATMOSPHERIC CHEMISTRY AND  
961 PHYSICS, 13, 7053-7074, 10.5194/acp-13-7053-2013, 2013.
- 962 Zheng, C. W., Zhao, C. F., Zhu, Y. N., Wang, Y., Shi, X. Q., Wu, X. L., Chen, T. M.,  
963 Wu, F., Qiu, Y. M.: Analysis of influential factors for the relationship between  
964 PM<sub>2.5</sub> and AOD in Beijing, ATMOSPHERIC CHEMISTRY AND PHYSICS, 17,  
965 13473-13489, 10.5194/acp-17-13473-2017, 2017.
- 966
- 967

968  
 969  
 970  
 971  
 972  
 973  
 974  
 975  
 976 Table 1. O<sub>3</sub> column concentration, temperature, relative humidity, daytime clear-sky  
 977 fraction and respective standard deviation for different seasons (spring: March, April  
 978 and May; summer: June, July and August; autumn: September, October and  
 979 November; winter: December, January and February).

---

| Season | O <sub>3</sub> column (DU) | Temperature (°C) | Relative humidity (%) | Clear-sky fraction(%) |
|--------|----------------------------|------------------|-----------------------|-----------------------|
| Spring | 355±37                     | 16±7.8           | 33±18                 | 41                    |
| Summer | 310±24                     | 28±4.2           | 57±18                 | 36                    |
| Autumn | 304±23                     | 16±7.4           | 46±21                 | 42                    |
| Winter | 347±28                     | 0.53±4.2         | 30±18                 | 41                    |

---

980  
 981  
 982  
 983  
 984  
 985  
 986  
 987  
 988

989

990

991

992

993

994 Table 2. Instruments deployed in the field campaign undertaken in August 2012 and  
 995 used for data analysis.

| Parameters                                  | Measurement technique  | Time resolution | Detection limit | Accuracy |
|---|------------------------|-----------------|-----------------|----------|
| j(O <sup>1</sup> D) and j(NO <sub>2</sub> ) | Spectroradiometer      | 10 s            | /               | ± 10%    |
| O <sub>3</sub>                              | UV photometry          | 60 s            | 0.5 ppbv        | ± 5%     |
| NO  | Chemiluminescence      | 60 s            | 60 pptv         | ± 20%    |
| NO <sub>2</sub>                             | Chemiluminescence      | 60 s            | 300 pptv        | ± 20%    |
| CO  | IR photometry          | 60 s            | 4 ppb           | ± 5%     |
| SO <sub>2</sub>                             | Pulsed UV fluorescence | 60 s            | 0.1 ppbv        | ± 5%     |
| HCHO  | Hantzsch fluorimetry   | 60 s            | 25 pptv         | ± 5%     |
| VOCs  | GC-FID/MS              | 1 h             | 20-300 pptv     | ± 15~20% |

996

997

998

999

1000

1001

1002

1003

1004

1005

1006  
 1007  
 1008  
 1009  
 1010  
 1011  
 1012 Table 3. Slope, intercept and the square of correlation coefficient ( $r^2$ ) of linear fits of  
 1013 correlation between  $j(O^1D)$  and AOD for each ozone column class at AOD smaller  
 1014 than 0.7.

| $O_3$ column<br>(DU) | SZA=30°                      |                                  |       | SZA=60°                      |                                  |       |
|----------------------|------------------------------|----------------------------------|-------|------------------------------|----------------------------------|-------|
|                      | Slope<br>( $10^{-6}s^{-1}$ ) | Intercept<br>( $10^{-6}s^{-1}$ ) | $r^2$ | Slope<br>( $10^{-6}s^{-1}$ ) | Intercept<br>( $10^{-6}s^{-1}$ ) | $r^2$ |
| 300-330              | -6.2±1.5                     | 26±1                             | 0.34  | -4.2±0.4                     | 7.7±0.3                          | 0.41  |
| 330-360              | -6.5±1.4                     | 23±1                             | 0.40  | -5.0±0.3                     | 7.1±0.2                          | 0.52  |
| 360-390              | -9.5±1.6                     | 21±1                             | 0.52  | -6.9±0.6                     | 7.6±0.3                          | 0.66  |

1015  
 1016  
 1017  
 1018  
 1019  
 1020  
 1021  
 1022  
 1023  
 1024  
 1025

1026  
 1027  
 1028  
 1029  
 1030  
 1031  
 1032  
 1033   Table 4. Slope, intercept and the square of correlation coefficient ( $r^2$ ) of linear fits of  
 1034   correlation between  $j(\text{NO}_2)$  and AOD for each ozone column class at AOD smaller  
 1035   than 0.7.

| $\cos(\text{SZA})$ | Slope ( $10^{-3} \text{ s}^{-1}$ ) | Intercept ( $10^{-3} \text{ s}^{-1}$ ) | $r^2$ |
|--------------------|------------------------------------|--|-------|
| 0-0.2              | -1.3±0.1                           | 1.5±0.0                                | 0.52  |
| 0.2-0.4            | -2.4±0.1                           | 3.4±0.0                                | 0.41  |
| 0.4-0.6            | -3.2±0.1                           | 5.5±0.0                                | 0.49  |
| 0.6-0.8            | -2.1±0.1                           | 7.2±0.1                                | 0.38  |
| 0.8-1.0            | -1.8±0.1                           | 8.1±0.1                                | 0.26  |

1036  
 1037  
 1038  
 1039  
 1040  
 1041  
 1042  
 1043  
 1044  
 1045  
 1046  
 1047

1048

1049

1050

1051 Table 5. The fitting parameters  $a_1-a_6$  and determination coefficients of E5 for  $j(\text{NO}_2)$ .

| $a_1$            | $a_2$           | $a_3$        | $a_4$           | $a_5$           | $a_6$          | $r^2$ |
|------------------|-----------------|--------------|-----------------|-----------------|----------------|-------|
| $\times 10^{-3}$ |                 |              |                 |                 |                |       |
| $-0.46 \pm 0.05$ | $-2.0 \pm 0.03$ | $13 \pm 0.2$ | $0.22 \pm 0.01$ | $0.32 \pm 0.05$ | $-4.0 \pm 0.1$ | 0.96  |

1052

1053

1054

1055

1056 Table 6. The fitting parameters  $a_1-a_6$  and determination coefficients of E6 for  $j(\text{O}^1\text{D})$ 

1057 at ozone column range = 300-330 DU.

| $a_1$            | $a_2$           | $a_3$          | $a_4$           | $a_5$          | $a_6$      | $r^2$ |
|------------------|-----------------|----------------|-----------------|----------------|------------|-------|
| $\times 10^{-6}$ |                 |                |                 |                |            |       |
| $1.1 \pm 0.3$    | $0.58 \pm 0.17$ | $-8.7 \pm 0.9$ | $0.63 \pm 0.05$ | $-7.5 \pm 0.3$ | $43 \pm 1$ | 0.96  |

1058

1059

1060

1061

1062

1063

1064

1065      Table 7. Mean and standard deviation of observed data during daytime (6:00–18:00)  
 1066      for A day and B day.

| Observed data                              | A day: August 21, 2012                      | B day: August 26, 2012                      |
|--|---|---|
| AOD  | $0.21 \pm 0.05$                             | $3.2 \pm 0.4$                               |
| PM <sub>2.5</sub> ( $\mu\text{g m}^{-3}$ ) | $22 \pm 9$                                  | $125 \pm 16$                                |
| O <sub>3</sub> column (Du)                 | $302 \pm 3$                                 | $301 \pm 3$                                 |
| Temperature( $^{\circ}\text{C}$ )          | $28 \pm 3$                                  | $28 \pm 3$                                  |
| Relative humidity (%)                      | $48 \pm 10$                                 | $55 \pm 12$                                 |
| j(O <sup>1</sup> D)( $\text{s}^{-1}$ )     | $1.6 \times 10^{-5} \pm 1.2 \times 10^{-5}$ | $6.9 \times 10^{-6} \pm 5.2 \times 10^{-6}$ |
| j(NO <sub>2</sub> )( $\text{s}^{-1}$ )     | $5.4 \times 10^{-3} \pm 2.9 \times 10^{-3}$ | $2.9 \times 10^{-3} \pm 1.7 \times 10^{-3}$ |
| O <sub>3</sub> (ppb)                       | $40 \pm 17$                                 | $87 \pm 53$                                 |
| NO <sub>2</sub> (ppb)                      | $11 \pm 5$                                  | $25 \pm 10$                                 |
| CO (ppm)                                   | $0.24 \pm 0.05$                             | $0.85 \pm 0.14$                             |
| VOC reactivity ( $\text{s}^{-1}$ )         | $3.0 \pm 0.7$                               | $6.4 \pm 1.7$                               |
| HCHO (ppb)                                 | $2.7 \pm 1.1$                               | $7.4 \pm 1.9$                               |

1067  
 1068  
 1069  
 1070  
 1071  
 1072  
 1073  
 1074

1075 Table 8. Monthly mean and standard deviation of observed data during daytime  
 1076 (6:00–18:00) under the condition of AOD less than 1 and larger than 1 in August 2012

| Observed data                              | AOD<1                                       | AOD>1                                       |
|--|---|---|
| AOD  | $0.43 \pm 0.24$                             | $2.0 \pm 0.8$                               |
| PM <sub>2.5</sub> ( $\mu\text{g m}^{-3}$ ) | $26 \pm 12$                                 | $77 \pm 47$                                 |
| O <sub>3</sub> column (Du)                 | $303 \pm 4$                                 | $302 \pm 5$                                 |
| Temperature(°C)                            | $30 \pm 4$                                  | $29 \pm 4$                                  |
| Relative humidity (%)                      | $42 \pm 16$                                 | $57 \pm 13$                                 |
| j(O <sup>1</sup> D)(s <sup>-1</sup> )      | $1.6 \times 10^{-5} \pm 1.1 \times 10^{-5}$ | $1.0 \times 10^{-5} \pm 0.7 \times 10^{-5}$ |
| j(NO <sub>2</sub> )(s <sup>-1</sup> )      | $5.6 \times 10^{-3} \pm 2.4 \times 10^{-3}$ | $3.8 \times 10^{-3} \pm 1.7 \times 10^{-3}$ |
| O <sub>3</sub> (ppb)                       | $52 \pm 34$                                 | $68 \pm 46$                                 |
| NO <sub>2</sub> (ppb)                      | $16 \pm 7.8$                                | $24 \pm 9$                                  |
| CO (ppm)                                   | $0.47 \pm 0.20$                             | $0.95 \pm 0.47$                             |
| VOC reactivity (s <sup>-1</sup> )          | $4.3 \pm 1.7$                               | $6.2 \pm 2.2$                               |
| HCHO (ppb)                                 | $4.0 \pm 1.4$                               | $6.5 \pm 1.9$                               |

1077  
 1078  
 1079  
 1080  
 1081  
 1082  
 1083  
 1084  
 1085

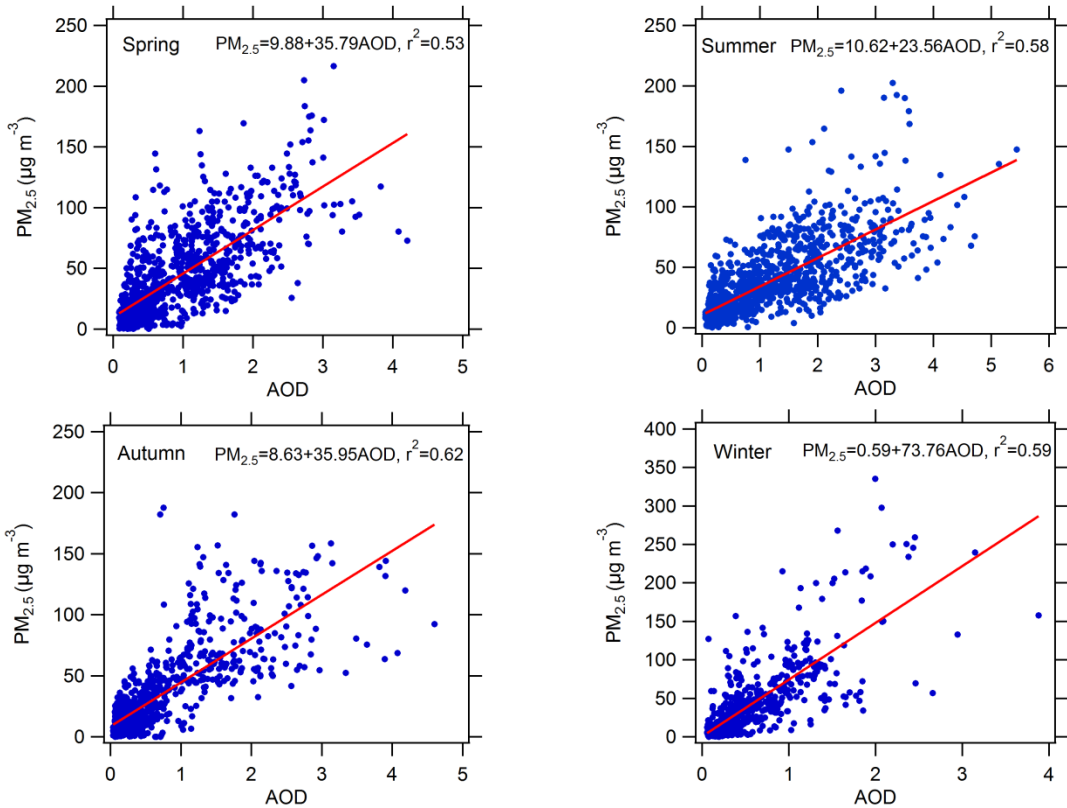


Figure 1. Scatter plots between AOD at 380nm and  $\text{PM}_{2.5}$  in four different seasons.

The slope, intercept and determination coefficient ( $r^2$ ) were calculated.

1086

1087

1088

1089

1090

1091

1092

1093

1094

1095

1096

1097

1098

1099

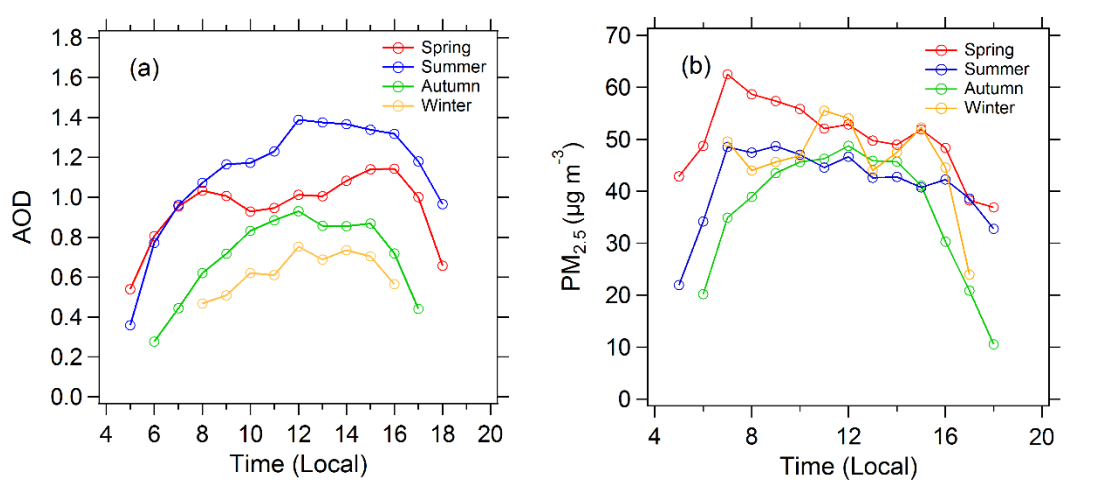
1100

1101

1102

1103

1104



1105

Figure 2. Diurnal cycles of (a) mean AOD and (b) mean  $\text{PM}_{2.5}$  in the four seasons

1106 under cloudless conditions.

1108

1109

1110

1111

1112

1113

1114

1115

1116

1117

1118

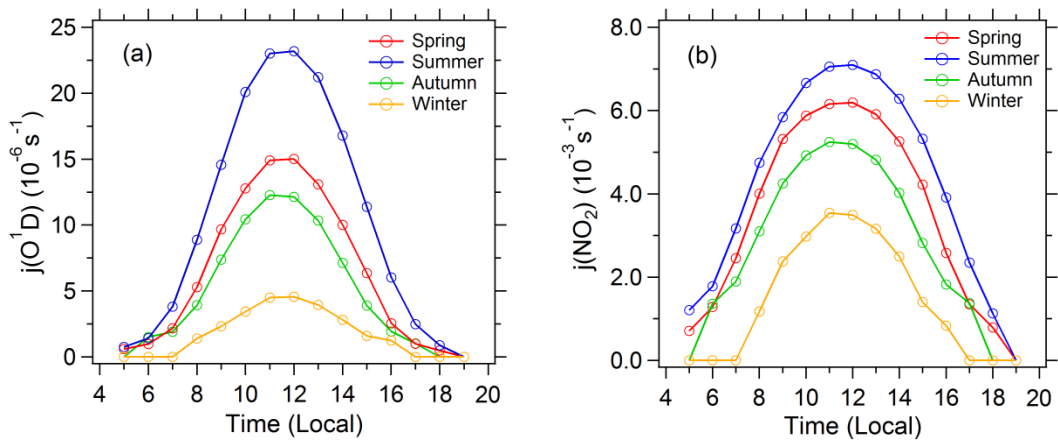
1119

1120

1121

1122

1123



1124

1125 Figure 3. Diurnal cycles of (a) mean  $j(O^1D)$  and (b) mean  $j(NO_2)$  in the four seasons

1126 under cloudless conditions.

1127

1128

1129

1130

1131

1132

1133

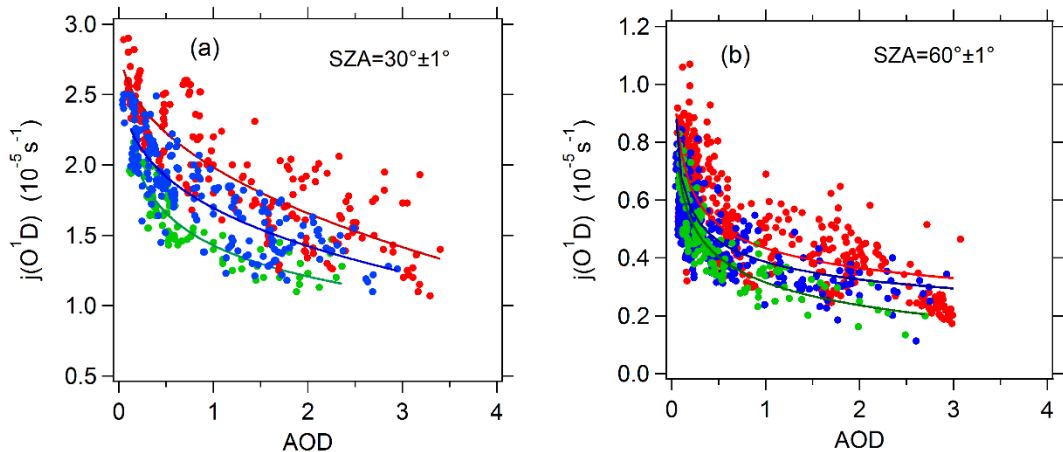
1134

1135

1136

1137

1138



1139

1140

1141 Figure 4. Dependence of  $j(O^1D)$  on AOD (380nm) at SZA of (a)  $30^\circ$  and (b)  $60^\circ$  and  
 1142 at different classes of ozone column concentration: 300-330 DU (red), 330-360 DU  
 1143 (blue), and 360-390 DU (green). The full lines are fitted by exponential function.

1144

1145

1146

1147

1148

1149

1150

1151

1152

1153

1154

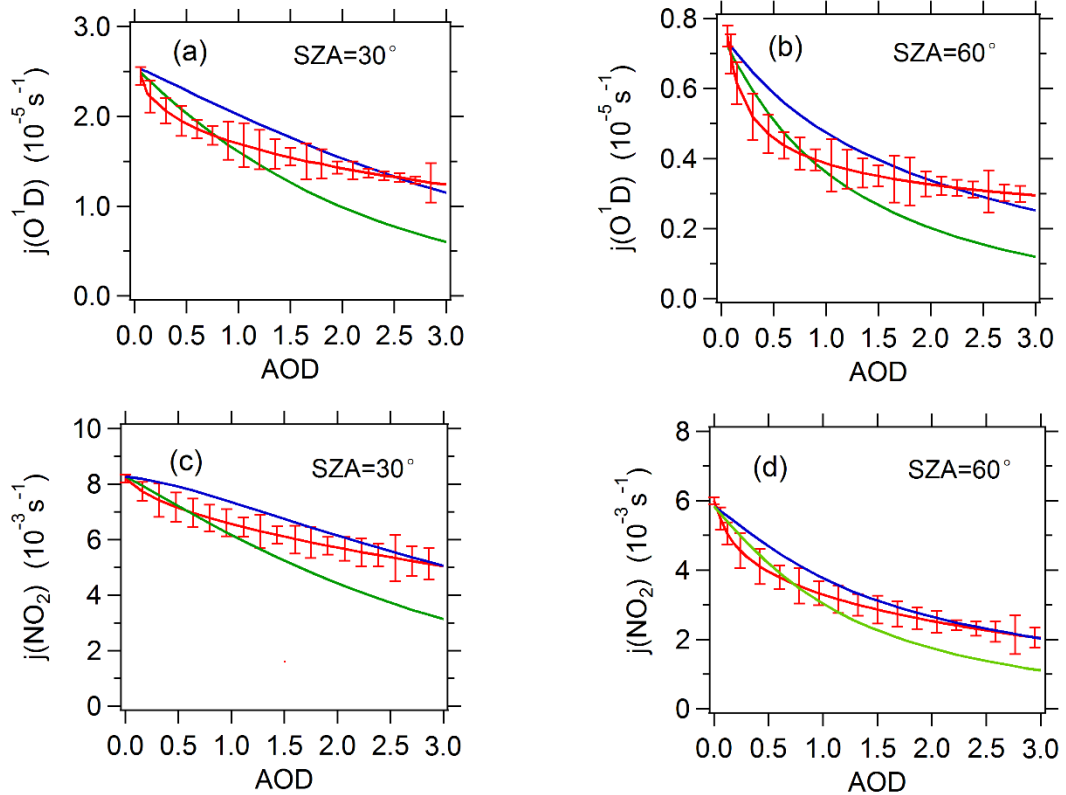
1155

1156

1157

1158

1159



1160

1161 Figure 5. The relationship between observed or TUV-simulated photolysis

1162 frequencies and AOD (380nm) at SZA of  $30^\circ$  and  $60^\circ$ . For  $j(O^1D)$ , total ozone

1163 column classification of 330-360 DU is chosen. The red line represents observed

1164 average photolysis frequencies; the blue line and green line represents TUV-simulated

1165 average photolysis frequencies at SSA of 0.95 and 0.85 respectively.

1166

1167

1168

1169

1170

1171

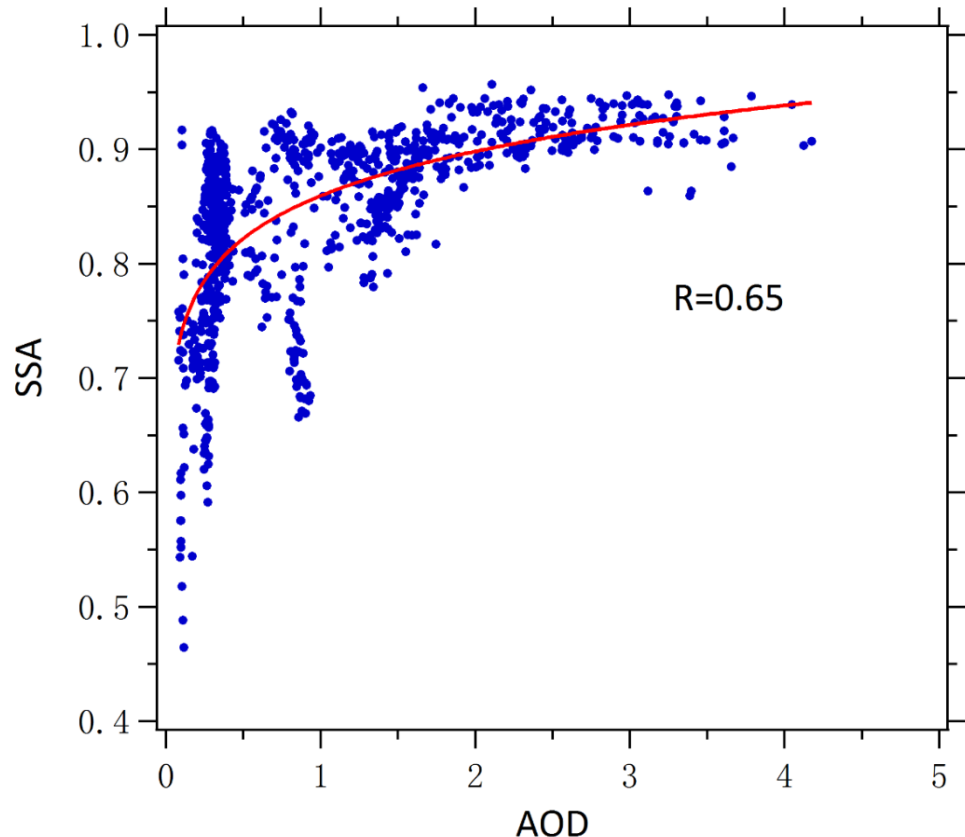
1172

1173

1174

1175

1176



1177

1178 Figure 6. Correlation between SSA and AOD (380nm) observed in August 2012.

1179

1180

1181

1182

1183

1184

1185

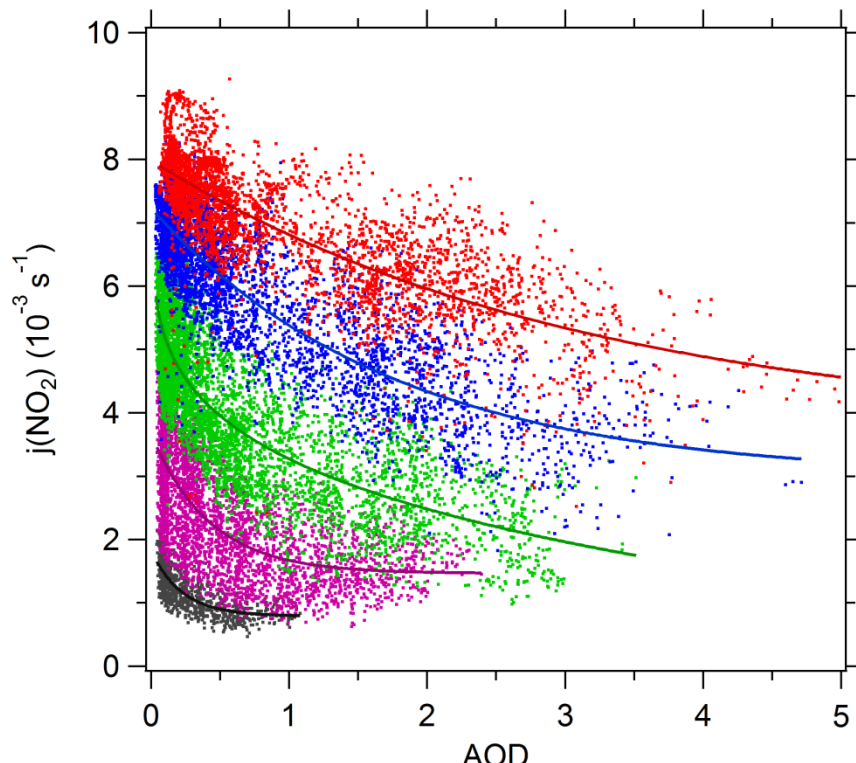
1186

1187

1188

1189

1190



1191

1192 Figure 7. Dependence of  $j(\text{NO}_2)$  on AOD (380nm) at different SZA classes. The  
 1193 classes of  $\cos(\text{SZA})$  are 0–0.2 (black), 0.2–0.4 (purple), 0.4–0.6 (green), 0.6–0.8  
 1194 (blue), and 0.8–1 (red). The full lines are fitted by exponential function.

1195

1196

1197

1198

1199

1200

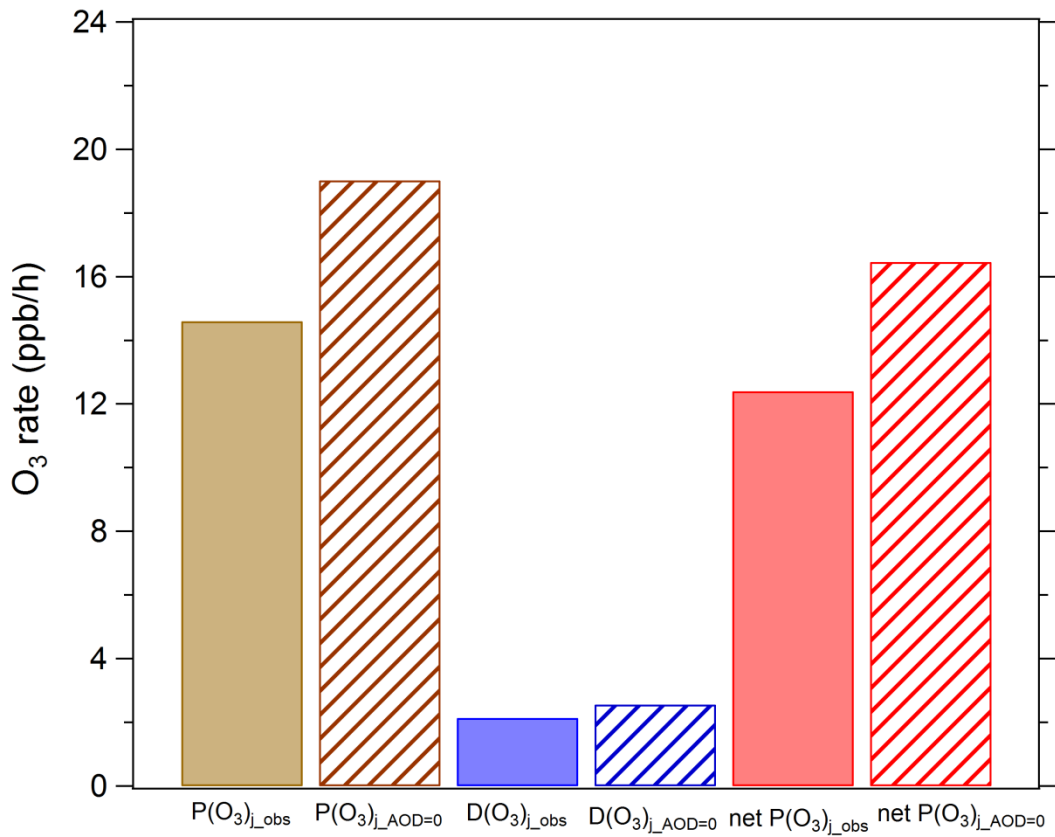
1201

1202

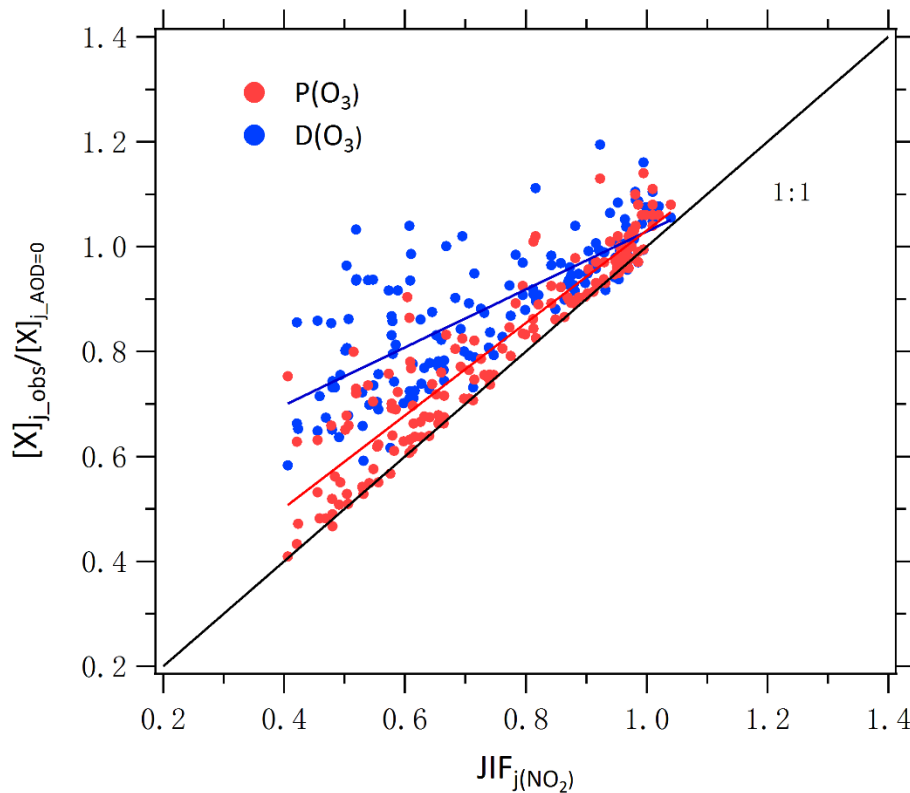
1203

1204

1205



1206  
 1207     Figure 8. Mean daytime ozone production and loss terms in August 2012.  $P(O_3)_{j\_obs}$ ,  
 1208      $D(O_3)_{j\_obs}$  and net  $P(O_3)_{j\_obs}$  represents ozone production rate, ozone loss rate, and net  
 1209     ozone production rate under observed photolysis frequencies;  $P(O_3)_{j\_AOD=0}$ ,  $D(O_3)$   
 1210      $_{j\_AOD=0}$  and net  $P(O_3)_{j\_AOD=0}$  represents ozone production rate, ozone loss rate, and net  
 1211     ozone production rate under calculated photolysis frequencies when AOD is equal to  
 1212     0.  
 1213  
 1214  
 1215  
 1216  
 1217  
 1218



1219

1220 Figure 9. Correlation between  $P(O_3)_{j\_obs}/P(O_3)_{j\_AOD=0}$  (or  $D(O_3)_{j\_obs}/D(O_3)_{j\_AOD=0}$ ) and  
1221 JIF of  $j(NO_2)$ . Single data point represent daytime hourly mean value.

1222

1223

1224

1225

1226

1227

1228

1229

1230

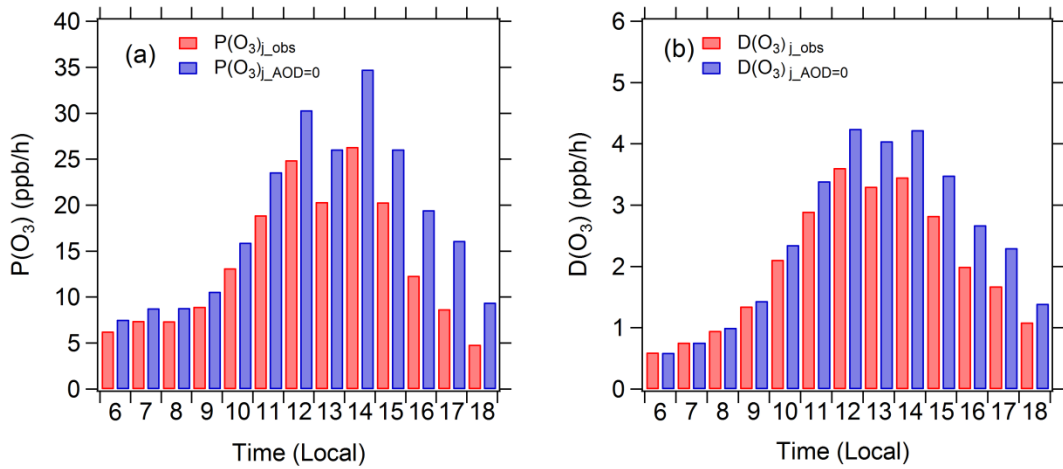
1231

1232

1233

1234

1235



1236

1237 Figure 10. Diurnal profiles of mean  $P(O_3)_{j\_obs}$ ,  $P(O_3)_{j\_AOD=0}$ ,  $D(O_3)_{j\_obs}$ , and

1238  $D(O_3)_{j\_AOD=0}$  in August 2012 under clear-sky conditions.

1239

1240

1241

1242

1243

1244

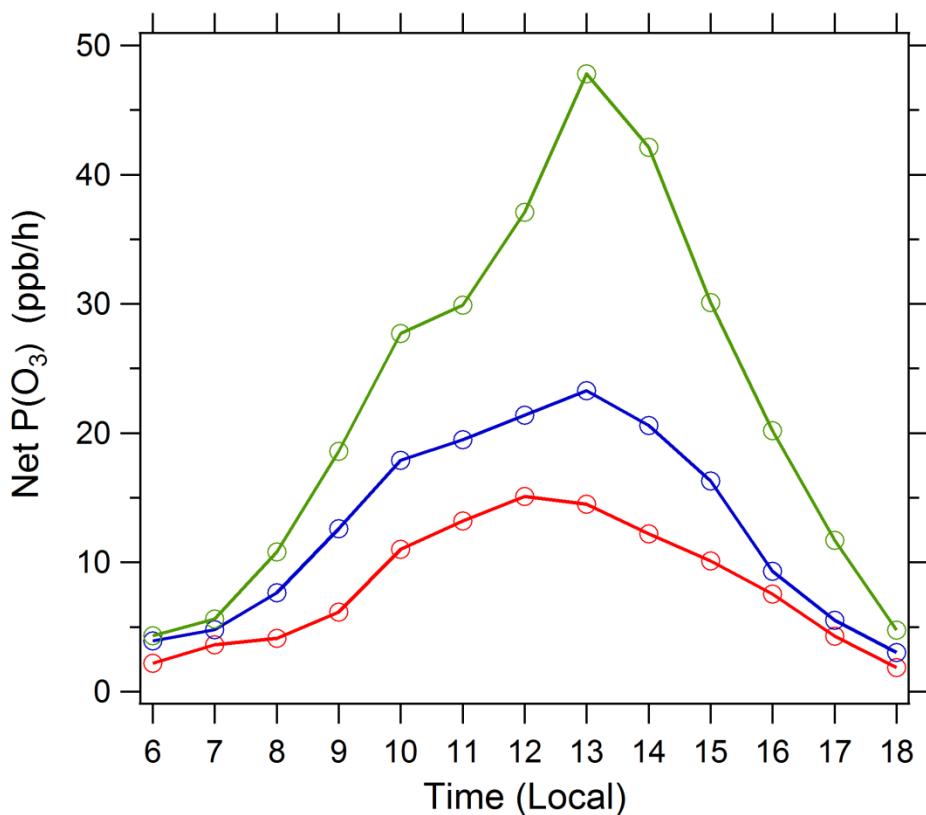
1245

1246

1247

1248

1249



1250

1251 Figure 11. Diurnal profile of net P(O<sub>3</sub>) simulated by the box model. Three cases are  
 1252 displayed: (1) A day (red circles): August 21, 2012 with low AOD level and high  
 1253 photolysis frequencies; (2) B day (blue circles): August 26, 2012 with high AOD level  
 1254 and low photolysis frequencies; and (3) the photolysis frequencies of B day adjusted  
 1255 to the level of A day with other conditions unchanged (green circles). The specific  
 1256 conditions of A day and B day are listed in Table 7.

1257

1258

1259

1260

1261

1262

1263

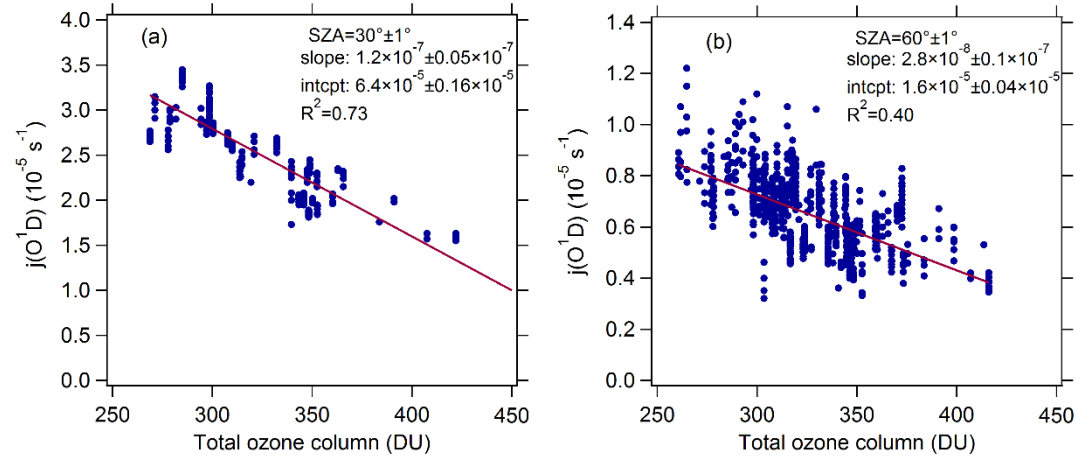
1264

1265 Supporting information

1266

1267

1268



1269

1270 Figure S1. Dependence of  $j(O^1D)$  on AOD (380nm) at low AOD level ( $AOD < 0.3$ ) and  
1271 SZA of (a)  $30^\circ \pm 1^\circ$  and (b)  $60^\circ \pm 1^\circ$ , respectively.

1272

1273

1274

1275

1276

1277

1278

1279

1280

1281

1282

1283

1284

1285

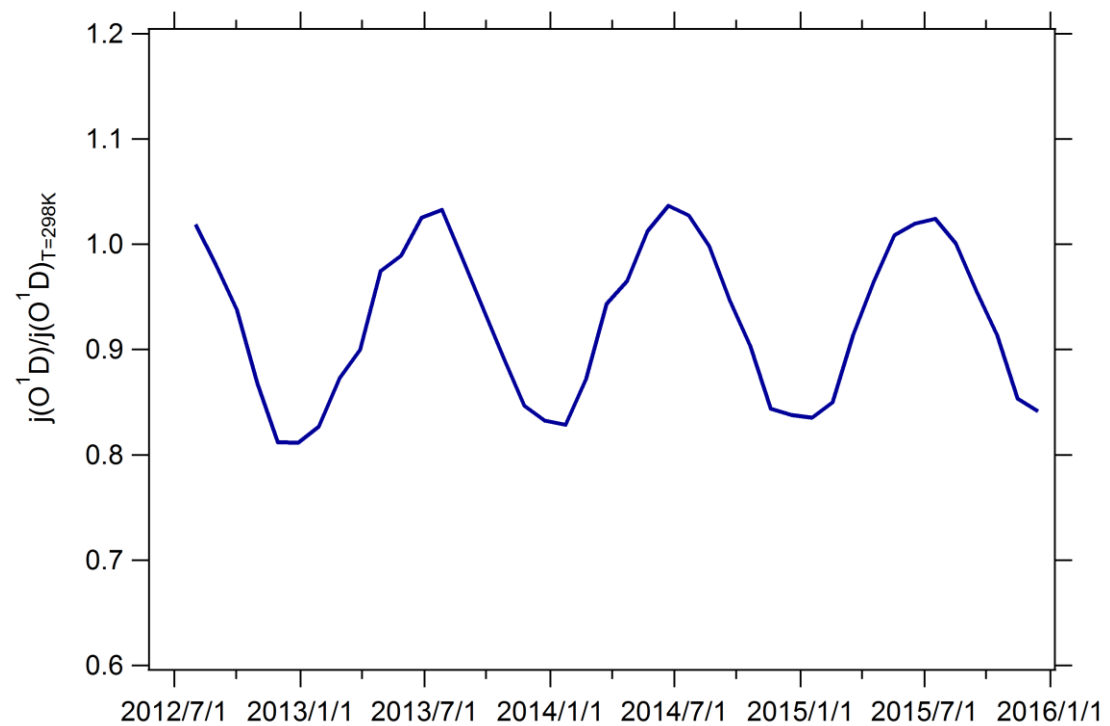
1286

1287

1288

1289

1290



1291

1292 Figure S2. The time series of the monthly mean ratio of  $j(O^1D)$  to  $j(O^1D)_{T=298K}$

1293  $(j(O^1D)/j(O^1D)_{T=298K})$  from August 2012 to December 2015.